Biochimica et Biophysica Acta 1838 (2014) 1985–1999

Contents lists available at ScienceDirect

Biochimica et Biophysica Acta

journal homepage: www.elsevier.com/locate/bbamem

Peptide:lipid ratio and membrane surface charge determine the mechanism of action of the antimicrobial peptide BP100. Conformational and functional studies

Mariana C. Manzini [a], Katia R. Perez [b], Karin A. Riske [b], José C. Bozelli Jr. [a], Talita L. Santos [c], Marcia A. da Silva [a], Greice K.V. Saraiva [a], Mario J. Politi [a], Ana P. Valente [c], Fábio C.L. Almeida [c], Hernan Chaimovich [a], Magali A. Rodrigues [d], Marcelo P. Bemquerer [d], Shirley Schreier [a,*], Iolanda M. Cuccovia [a,*]

[a] Department of Biochemistry, Institute of Chemistry, University of São Paulo, São Paulo, C.P. 26077, 05513–970, Brazil
[b] Department of Biophysics, Federal University of São Paulo, São Paulo, 04044–020, Brazil
[c] Nuclear Magnetic Resonance National Center, Institute of Medical Biochemistry, Federal University of Rio de Janeiro, Rio de Janeiro, Brazil
[d] Embrapa Recursos Genéticos e Biotecnologia, Parque Estação Biológica, P.O. Box 02372, 70770–917, Brasília, Brazil

ARTICLE INFO

Article history:
Received 7 November 2013
Received in revised form 21 March 2014
Accepted 5 April 2014
Available online 15 April 2014

Keywords:
BP100
Antimicrobial peptide
CD
NMR
Zeta potential
Model membrane leakage

ABSTRACT

The cecropin-melittin hybrid antimicrobial peptide BP100 (H-KKLFKKILKYL-NH2) is selective for Gram-negative bacteria, negatively charged membranes, and weakly hemolytic. We studied BP100 conformational and functional properties upon interaction with large unilamellar vesicles, LUVs, and giant unilamellar vesicles, GUVs, containing variable proportions of phosphatidylcholine (PC) and negatively charged phosphatidylglycerol (PG). CD and NMR spectra showed that upon binding to PG-containing LUVs BP100 acquires α-helical conformation, the helix spanning residues 3–11. Theoretical analyses indicated that the helix is amphipathic and surface-seeking. CD and dynamic light scattering data evinced peptide and/or vesicle aggregation, modulated by peptide:lipid ratio and PG content. BP100 decreased the absolute value of the zeta potential (ζ) of LUVs with low PG contents; for higher PG, binding was analyzed as an ion-exchange process. At high salt, BP100-induced LUVS leakage requires higher peptide concentration, indicating that both electrostatic and hydrophobic interactions contribute to peptide binding. While a gradual release took place at low peptide:lipid ratios, instantaneous loss occurred at high ratios, suggesting vesicle disruption. Optical microscopy of GUVs confirmed BP100-promoted disruption of negatively charged membranes. The mechanism of action of BP100 is determined by both peptide:lipid ratio and negatively charged lipid content. While gradual release results from membrane perturbation by a small number of peptide molecules giving rise to changes in acyl chain packing, lipid clustering (leading to membrane defects), and/or membrane thinning, membrane disruption results from a sequence of events – large-scale peptide and lipid clustering, giving rise to peptide-lipid patches that eventually would leave the membrane in a carpet-like mechanism.

1. Introduction

Antimicrobial resistance to antibiotics is currently a serious global heath issue. The alarming growth of microorganisms resistance to conventional antibiotics and the stagnation in the development of antibiotics with new mechanisms of action led to publication by the World Health Organization (WHO) of a book pointing at strategies to prevent this growth and emphasizing the urgent need for the development of antibiotics with new mechanisms of action [1]. The use of antimicrobial peptides (AMPs) has been considered as a possible solution. AMPs display a wide spectrum of action against Gram-positive and Gram-negative bacteria, fungi, protozoa, virus, and mammalian cells [2–7]. In addition, they usually act in the timescale of minutes over multiple macromolecular targets, *e.g.* membranes, nucleic acids, mitochondria, proteins, rendering it difficult for microorganisms to develop resistance [5,8–10].

Several mechanisms have been proposed for the action of AMPs at the membrane level. Among those, the most frequently discussed are the barrel-stave [11–13], the toroidal pore [14], and the carpet model [15–17]. More recently, a model involving lipid clustering has also been proposed [18–20]. For a detailed description of the existing models, see ref. [7].

Among the AMPs, two peptides have been extensively studied, cecropin A and melittin. Merrifield and coworkers focus on obtaining shorter hybrid peptides of these AMPs aiming at increasing their effectivess and decreasing the damaging effects on host membranes

* Corresponding authors. Tel.: +55 11 3091 2177.
E-mail addresses: schreier@iq.usp.br (S. Schreier), imcuccov@iq.usp.br (I.M. Cuccovia).

http://dx.doi.org/10.1016/j.bbamem.2014.04.004
0005-2736/

(high therapeutic index, TI, which is the ratio between toxic and antimicrobial concentrations) [21,22, for a review see ref. 23]. Another approach proposes the use of synthetic combinatorial libraries to engineer AMPs of high TI [24]. In this context, Badosa and collaborators [25] identified the cationic eleven-residue hybrid peptide BP100 (H-KKLFKKILKYL-NH_2), whose residues 2–7 correspond to residues 3–8 of cecropin A and whose residues 8–11 correspond to residues 6–9 of melittin, V^8 being replaced by Y. *In vitro*, BP100 is highly active and selective toward Gram-negative bacteria, including the phytopathogenic bacterium *E. amylovora*. The peptide minimal inhibitory concentration (MIC) for several Gram-negative bacteria is between 2.5 and 5 μM [25–27]). Furthermore, the peptide exhibits low cytotoxicity against erythrocytes and fibroblasts, and little susceptibility to protease degradation [26,28].

Although the action of BP100 involves interaction with the membrane, the mechanism is not completely understood at a molecular level. Atomic force microscopy shows that at the MIC, BP100 progressively destroys the *E. coli* cell envelope, leading to leakage of cytoplasmic contents [26,27]. Under conditions where *E. coli* cells are exposed to BP100 for long periods (≥2 h) and high peptide concentrations (≥MIC), vesicle-like structures are formed and alterations occur in the surface roughness. Zeta potential measurements of *E. coli* incubated with increasing BP100 concentrations show a correlation between the MIC (3 μM) and membrane surface charge neutralization [26]. In addition, BP100 labeled with fluorescein-isothiocyanate translocates into the cytosol of walled plant cells [28]. Furthermore, designed constructs of BP100 fused to other peptides can transport cargoes into plant cells [29,30].

Fluorescence and surface plasmon resonance (SPR) studies of model membranes show that electrostatic interactions are important for BP100 binding, as evidenced by its strong selectivity towards negatively charged as compared to zwitterionic membranes [27,28]. Moreover, the peptide was also found to bind to and neutralize lipopolysaccharide (LPS) and lipoteichoic acids (LTA), the negatively-charged molecules in the cell envelope of Gram-negative and Gram-positive bacteria, respectively [27]. For negatively charged membranes, at high peptide:lipid ratios, membrane saturation was observed and the effect correlates with BP100-induced vesicle permeabilization, membrane electroneutrality, and vesicle aggregation. In addition, fluorescence studies show that BP100 translocates across lipid bilayers at both high and low peptide:lipid ratios [28]. Brownian dynamics (BD) simulations of a coarse-grained model of BP100 confined within phospholipid bilayers point to the acquisition of α-helical conformation by the peptide [31]. In agreement with the calculations, circular dichroism (CD) spectra of the peptide show acquisition of α-helical conformation upon binding to model membranes containing negatively charged phospholipids, although the α-helical content was not calculated [27,32,33]. In a study that came out early this year, Wadhwani and coworkers examined the conformation, membrane alignment, and dynamical behavior of BP100 in DMPC:DPMG bilayers making use of oriented circular dichroism (OCD) and solid-state ^{15}N NMR. The data indicated that the BP100 helix is oriented roughly parallel to the membrane surface and that the peptide is rotating fast around the bilayer normal [34].

Here we present a comprehensive study of the interaction between BP100 and model membranes (LUVs and GUVs) of variable lipid composition. We examined conformational aspects by performing theoretical prediction of BP100 conformation and calculating the peptide hydrophobicity and hydrophobic moment; experimental approaches employed CD and NMR spectroscopies. Dynamic light scattering was used to investigate the peptide effect on vesicle size and determination of ζ from electrophoretic mobilities, provided information about its effect upon membrane electrical properties. BP100-promoted leakage of fluorescent probes from the aqueous inner compartment of LUVs was studied at low and high ionic strength. Finally, the peptide-membrane interaction was also investigated by optical microscopy of GUVs. The results provided evidence for a dependence of the mechanism of action of BP100 on peptide:lipid molar ratio and on the membrane content of negatively charged phospholipid.

2. Materials and methods

2.1. Materials

1-Palmitoyl-2-oleoyl-*sn*-glycero-3-phosphocholine, (POPC), L-α-phosphatidylglycerol (egg, sodium salt) (PG) and 1-palmitoyl-2-oleoyl-*sn*-glycero-3-[phospho-rac-(1′-glycerol)] sodium salt (POPG), were from Avanti Polar Lipids (Alabaster, AL). Egg phosphatidylcholine (PC) was extracted from egg yolk and purified as previously described [35]. Sephadex G-25 medium, Sephadex LH-20, sucrose, glucose, tris-hydroxymethylaminomethane (Tris), methyl viologen (MV), 1,3,6,8-pyrenetetrasulfonic acid tetrasodium salt (PTS), polidocanol (polyoxyethylene (9) lauryl ether), 2,2,2-trifluoroethanol (TFE), 4-methylpiperidine (4-MP), triisopropylsilane (TIPS), diisopropylcarbodiimide (DIC), 1-hydroxybenzotriazole (HOBt), trimethylsilyl propionate (TSP), and α-cyano-4-hydroxycinnamic acid were from Sigma-Aldrich (St Louis, MO). 2-Propanol, methanol and trifluoracetic acid (TFA) were from VETEC (Rio de Janeiro, Brazil). Dichloromethane (DCM) and acetonitrile (ACN) were from J.T. Baker (Xalostoc, Mexico). 2-cyano-2-(hydroxyimino) ethyl acetate (Oxyma) was from Merck (Darmstadt, Germany). The amino acid derivatives (Fmoc-amino acids) and the resin utilized for peptide synthesis were from Peptides International (Louisville, KY). N,N-dimethylformamide (DMF) was from SYNTH (São Paulo, Brazil) and was dried under KOH and freshly distilled before use. 5(6)-carboxyfluorescein (CF) from Sigma-Aldrich (St Louis, MO), was purified as described by Ralston et al. [36] and the hydrophobic contaminants were eliminated using an LH-20 resin. The LH-20 resin was recovered by exhaustive washings with ethanol containing 10 mM HCl until elimination of the adsorbed contaminants and washed with pure ethanol. The recovered resin was maintained at room temperature until evaporation of the residual solvent, stored in the dry form, and reused when needed. The CF eluted from the LH-20 column was in the form of sodium salt. The CF concentration was determined from the absorbance at 492 nm [36] using a molar extinction coefficient of 7.5 x 10^4 M^{-1} cm^{-1} determined in 10 mM borate buffer, pH 9. Other reagents were of analytical grade and were used without further purification. MilliQ water was used in all studies.

2.2. Methods

2.2.1. Peptide synthesis

BP100 (H-KKLFKKILKYL-NH_2) was synthesized by the solid phase method [37,38], starting from "Rink-Amide-MBHA-Resin" (Peptides International, Louisville, KY), with a substitution degree of 0.52 mmol.g^{-1}. The deprotection reaction of the Fmoc group was performed with 25% (v/v) 4-MP/DMF for 30 min (two 15 min steps). The couplings for peptide bond formation were conducted with DIC/Oxyma [39] in DMF during 60 to 120 min.

The deprotection and coupling reactions were monitored with ninhydrin test [37,40]. After each deprotection and coupling step, the resin was washed three times with 2-propanol (or methanol) and DMF, in alternating mode. After the synthesis was completed, the final deprotection reaction and peptide cleavage from the resin were performed with 10 mL of a TFA:TIPS:water (90:5:5, v:v:v) solution for 90 min at room temperature. After four washings with cold diisopropyl ether, the supernatant was discharged and the peptide was extracted with water and freeze-dried.

The peptide was purified by reverse-phase chromatography and characterized by mass spectrometry. For purification, a semi-preparative column (Zorbax ODS 9.4 x 250 mm) from Agilent (Santa Clara, CA) was used. The chromatograph had an LC-10 pump, an SPD-10AV UV-visible detector, an FCV-10AL model solvent mixer unit, a DGU-14A degasser, and a manual Rheodyne injector (Bristol, CT). All accessories were

coupled to an SCL-10A system controller unit (Shimadzu, Kyoto, Japan). The gradient used was as follows: H_2O:ACN:TFA (95:5:0.1, v:v:v) for 5 min, followed by a linear gradient of H_2O:ACN:TFA (35:65:0.1, v:v:v) for 60 min. The detection was performed at 216 nm and 280 nm and the flow rate was 3.0 $mL.min^{-1}$, at room temperature. The identity and purity of the peptide were verified by MALDI-ToF mass spectrometry, using α-cyano-4-hydroxycinnamic acid as matrix. The spectra were acquired in an Ultraflex III ToF-ToF (Bruker Daltonics, Billerica, MA), in the reflected mode. Peptide fragmentation by MS/MS was conducted through the LIFT™ methodology [41].

Aqueous stock solutions of BP100 were prepared and the concentration was determined by measuring the absorbance of Tyr at 276 nm using a molar extinction coefficient of 1,450 M^{-1} cm^{-1}.

2.2.2. Preparation of small unilamellar vesicles (SUVs)

Stock solutions of different lipids in DCM or chloroform were added, at the desired molar ratios, to glass tubes. The solvent was eliminated under a N_2 flux and remaining traces were removed in a vaccum chamber. The dried films were suspended, by vigorous vortexing, in the desired aqueous solutions forming large multillamelar vesicles (MLV). SUVs were prepared by sonication of MLVs suspension in a G112SP1 Special Ultrasonic Cleaner, from Laboratory Supplies Company Inc., Hicksville, NY, immersed in an ice/water bath, at 80 Watts, for 20 min. The SUVs were used to saturate the Sephadex-G25 columns (0.8 x 20 cm) and were prepared always with the same lipid composition used in each experiment (at a total phospholipid concentration of 0.01 M) and in the same buffers used to elute the column.

2.2.3. Preparation of large unillamelar vesicles (LUVs)

Lipid films of variable composition were prepared as described above. The composition of the aqueous solutions used to prepare MLVs varied according to the experiments. The MLVs were subjected to five cycles of freeze-thawing by alternately using a bath of dry ice/ethanol and a water bath at 37 °C followed by extrusion through a LiposoFast extruder (Avestin Inc., Ottawa, Canada). The LUVs suspension was passed (21 passages) through two stacked membranes of polycarbonate Nucleopore Track-Etch filters (Whatman-GE Healthcare, Waukesha, WI) with 100 nm diameter pores, at room temperature.

For CD spectroscopy, LUVs were prepared in MilliQ water, pH 6.5, at a final lipid concentration of 20 mM. For NMR, LUVs were prepared in 15 mM Tris–HCl buffer, pH 7.4, containing 50 mM NaCl and 10% D_2O for lock, at a final lipid concentration of 42.7 mM.

For the D_h and U_E measurements LUVs (5 mM total lipid) were prepared in 10 mM Tris-HF buffer, pH 8.1. Tris-HF buffer was used to minimize electrode oxidation during the sequential measurements of U_E.

In the case of PTS-loaded LUV, the lipid films were hydrated with 0.5 mL of 1 mM PTS in water. The final lipid concentration was 17 mM. The PTS in the buk aqueous phase was removed by eluting ca. 0.5 mL of LUVs, on a Sephadex-G25 column (see **Section** 2.2.2) with 20 mM Tris–HCl buffer, pH 8.1. LUVs were collected in 1 mL at the column void volume (final phospholipid concentration *ca.* 2 mM, see **Section** 2.2.5) and the pool was maintained in an ice bath until use.

For preparation of CF-loaded LUVs, the lipid films were hydrated with 0.5 mL of 50 mM CF, in the sodium salt form, in 10 mM Tris–HCl buffer, pH 8.1, yielding a final lipid concentration of 17 mM. External CF was removed in a Sephadex-G 25 column (**Section** 2.2.2) by elution with 10 mM Tris–HCl buffer pH 8.1 and 300 mM NaCl [42]. The LUVs were collected in 2 mL, at the void volume, and the pool was maintained in an ice bath until use.

2.2.4. Determination of phospholipid concentration

The phospholipid concentration in the vesicle pool collected from the Sephadex G-25 column was determined from inorganic phosphate analysis using an adapted method of Rouser et al. [43]. Briefly, aliquots of the vesicles pools were added to glass tubes (previously cleaned with HCl 36 % and after with water) and the solvent completely evaporated at 120 °C. $HClO_4$ 70 % was added (0.4 mL), the tubes were capped with glass marbles and maintained in a heating block set at 180 °C for 1 h. After cooling, 1 mL of water and 0.4 mL of ammonium molibdate 1.25 % (w/v) were added to the tubes and vortexed. Then 0.4 mL of 3 % ascorbic acid (w/v) were added to each tube and vortexed immediately and vigorously. The tubes were maintained in a water bath at 100 °C for 10 min. The absorbance was read at 797 nm and phosphate concentration was calculated using a standard curve made with a 0.001 M KH_2PO_4 solution.

2.2.5. Circular dichroism studies

CD spectra were acquired at 20 °C in a Jasco J-720 spectropolarimeter (Tokyo, Japan). Samples were placed in 1.00 mm optical path quartz cells. The final spectra were the average of six scans, followed by subtracting the spectrum obtained under the same conditions of a sample without peptide. Spectra were scanned from 190 to 260 nm, at a rate of 20 $nm.min^{-1}$, 1 nm resolution, 8 s time response, using 2 nm slit. The initial peptide concentrations were 27.4 and 24.8 μM for the TFE and membrane experiments, respectively. Spectra were acquired for the free peptide and after addition of increasing TFE and LUV concentrations. The TFE content varied from 0 to 90% (v/v) and the lipid concentration from 0 to 1 mM.

The fraction of α-helical conformation acquired by the peptide was calculated using Chen´s equation (Eq. (1), ref. [44]):

$$[\theta]_{222nm} = (f_H - ik/N)^*[\theta]_{H\infty} \quad (1)$$

where $[\theta]_{222\ nm}$ is the mean residue molar ellipticity at 222 nm; $[\theta]_{H\infty}$ is the mean residue molar ellipticity for an infinite helix ($-39{,}500$ $deg.cm^2.dmol^{-1}$); f_H is the fraction of peptide in helical conformation; i is the number of helical segments (taken as 1 in the present study); N is the number of residues, and k is a constant that depends on λ, 2.57 at 222 nm.

2.2.6. NMR studies

NMR spectra were acquired in Avance III 600 and 800 MHz Bruker spectrometers at 25 °C, using a 5 mm probe. Stock solutions of 4 mM BP100 and 42.7 mM of total lipid for the LUVs were used; the concentrations of peptide and lipid in the samples are given in the captions of Fig. 3. ^1H spectra were acquired for the free peptide and after addition of increasing LUV concentrations. Spectra were acquired with 90° pulses around 10 μs and 1.2 s of repetition delay and sweep width of 12 ppm. All chemical shifts were referenced as described by Wishart et al. [45] using TSP. Watergate was used for water suppression [46]. TOCSY spectra were acquired at a mixing time of 60 ms using MLEV [47], with a spin-lock field of *ca.* 10 kHz, and spin-lock time of 60 ms. NOESY and ROESY spectra were acquired at 100 ms mixing time. Usually, ROESY experiments give better results when compared to NOESY for peptides whose correlation time falls in a regime where the product of the molecular correlation time and the Larmor frequency is close to unity. Both TOCSY and NOESY were acquired as 4096 x 512 complex points, using Watergate for water suppression [46] and States-TPPI for frequency discrimination in the indirect dimension. NMRPipe was used for spectra processing and NMRView for spectral analysis [48,49]. ^{13}C-HSQC and ^{15} N-SOFAST-HMQC spectra were also acquired using natural abundance, to help in the assignments in case of overlap [50].

2.2.7. Dynamic light scattering, zeta potential (ζ) and electrophoretic (U_E) mobility

The values of hydrodynamic diameter (D_h), zeta potential (ζ), and electrophoretic mobility (U_E) of LUVs were determined at 30 °C, in a quartz cuvette, using a Zetasizer Nano ZS light scattering apparatus equipped with a 633 nm laser, from Malvern (Worcestershire, UK). The U_E was measured using a dip cell electrode. ζ was calculated from

U_E values using Henry´s equation with Smoluchovski approximation. The buffer used for vesicle dilution was previously filtered through a Millipore membrane (Billerica, MA) of 0.22 μm pore diameter. Values of D_h and U_E were the average of three independent runs. The U_E of a standard sample was measured before and after each series of experiments to assure that the electrode sensitivity was maintained.

For the D_h and U_E measurements, 25 μL of LUVs (5 mM total lipid stock solution) were added to 1 mL buffer solution, yielding a phospholipid concentration of 125 μM. After measuring the initial values of D_h and U_E, aliquots of BP100 stock solutions were added at 10 min intervals and D_h, U_E, and ζ were determined.

2.2.8. PTS leakage from LUVs

PTS leakage was followed by adding 5 μL of 2 mM LUVs to 0.5 mL of 1 mM MV 14 mM Tris–HCl, pH 8.1, under stirring, at 30 °C. PTS fluorescence emission was measured at 400 nm using $\lambda_{ex} = 350$ nm. As PTS leaks from LUVs, its fluorescence decreases due to the presence of MV, a fluorescence quencher, in the external aqueous compartment. In aqueous solution, the fluorescence of 17 μM PTS decreased 85% in the presence of 1 mM MV in solution. In the presence of LUV, BP100 was added to the cuvette after 100 s, and the decrease in fluorescence intensity was recorded as a function of time. After 900 s, 10 μL of polidocanol 10% (w/w) were added to obtain complete vesicle leakage and maximum PTS quenching. The % of PTS leakage, after a defined time, was calculated according to Eq. (2):

$$\%\ \text{Leakage} = \frac{(I_0 - I_t)}{(I_0 - I_{tot})} x100 \quad (2)$$

where I_0 is the fluorescence intensity before addition of BP100, I_t is the fluorescence at a defined time after BP100 addition, and I_{tot} is the fluorescence after polidocanol addition. All fluorescence measurements were performed in a Hitachi F-2000 (Tokyo, Japan) fluorimeter using a 3 mL quartz cuvette with 10 mm optical path.

2.2.9. CF leakage from LUVs

The fluorescence of CF is self-quenched at high concentration. It was possible to analyze the BP100-induced leakage of CF from LUVs by monitoring the fluorescence increase at $\lambda_{em} = 520$ nm using $\lambda_{exc} = 490$ nm, at 700 V [51]. At zero time, an aliquot of CF-loaded LUVs (in general 5 μL of a 2 mM lipid solution), was added to a cuvette containing 10 mM Tris–HCl buffer, pH 8.1, 300 mM NaCl, reaching a total volume of 0.50 mL, under continuous stirring. The fluorescence was continuously recorded during 100 s; an aliquot of BP100 stock solution (200 μM, in water) was added and the fluorescence emission was followed for 3,000 s. At this time, 10 μL of polidocanol (10 % w/w) were added to disrupt all vesicles and obtain the maximum CF fluorescence. In general, aliquots of 5 to 50 μL of BP100 (2–40 μM) were added in each experiment. The leakage of CF was calculated making use of Eq. (3):

$$\%\ \text{Leakage} = \frac{(I_t - I_o)}{(I_{tot} - I_0)} x100 \quad (3)$$

where I_0 is the initial fluorescence intensity, before BP100 addition, I_t is the fluorescence at a choosen time after peptide addition, and I_{tot} is the fluorescence after polidocanol addition. All experiments were performed at 30 °C.

2.2.10. Optical microscopy studies of giant unilamellar vesicles (GUVs)

GUVs composed of POPC and POPC:POPG 70:30 (molar ratio) were prepared by the electroformation method [52,53]. Few microliters of a lipid solution in chloroform (2 $mg.mL^{-1}$) were spread on the surfaces of two glass slides coated with FTO (fluorine tin oxide) and the solvent was evaporated with a flux of N_2. The slides separated by a 2 mm Teflon frame were sealed to form a chamber which was filled with a 0.2 M sucrose solution. The slides were then connected to a function generator and an AC field of 1 V and 10 Hz was applied for 1 h.

The GUVs were observed by phase contrast with a Zeiss Axiovert 200 inverted optical microscope (Jena, Germany) equipped with a 63x objective and an AxioCam HSm digital camera from Zeiss (Jena, Germany). A home-made observation chamber filled with a solution of 50 μM BP100 in 0.2 M glucose was placed on the microscope stage. A small aliquot of the GUVs suspension was added and the observation was started after few seconds. Time sequences were recorded with the software Zeiss AxioVision. The osmolarities of the sucrose and glucose solution were matched throughout the measurements with a cryoscopic osmometer Osmomat Gonotec (Berlin, Germany). Experiments were performed at 25 °C.

3. Results

3.1. Conformational properties of BP100

Although presently the secondary structure of a protein/peptide cannot be predicted precisely based on its sequence, some dynamics calculations allow estimating the tendency of a given sequence to attain a specific structure. Making use of PSIPRED [54], a high tendency for BP100 to acquire helical conformation was predicted (not shown). According to the Schiffer-Edmundson helical wheel projection [55], BP100 could form an amphipathic α-helix as depicted in Scheme 1.

OCD and solid-state ^{15}N NMR data indicated that the BP100 helix is oriented roughly parallel to the membrane surface [34]. This observation was corroborated by calculating the peptide mean hydrophobicity (<H>) and mean hydrophobic moment (<μ_H>) making use of the formalism of Eisenberg et al. [56] for an amphipathic α-helix. The values of < H > and < μ_H > were found to be, respectively, −0.23 and 0.52, which characterizes BP100 as a surface-seeking amphipathic α-helix [56].

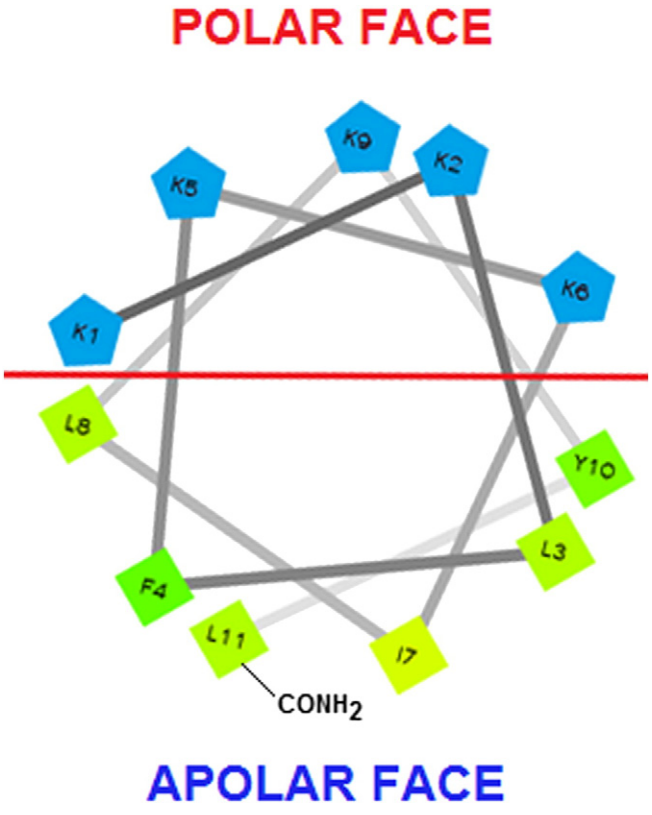

Scheme 1. Schiffer-Edmundson helical wheel projection indicating putative polar and apolar faces of BP100 amphipathic α-helix.

3.1.1. CD studies

To assess the conformational properties of BP100 in solution and upon binding to bilayers, we performed a comprehensive study of the peptide CD spectra as a function of lipid composition and lipid:peptide molar ratio. The far-UV CD spectrum of BP100 in aqueous solution exhibited a negative band centered at 197 nm, indicating that the peptide exists as an equilibrium of conformations (Fig. 1A). The spectra remained unchanged with peptide concentration (10 to 100 μM), suggesting that BP100 did not aggregate in this concentration range (not shown).

The tendency of a peptide to acquire secondary structure can be evaluated by addition of a structure-inducing agent, *e.g.* 2,2,2-trifluoroethanol (TFE) [57–59]. Increasing TFE concentration led to changes in the CD spectra of BP100, suggestive of a more ordered conformation (Fig. 1A). After saturation (≥40% TFE, Fig. 1B), the spectrum is characterized by a positive band at 192 nm and two negative bands at 207 and 222 nm, indicating that the peptide adopted α-helical conformation, in agreement with the PSIPRED prediction. At 90% TFE, making use of Chen´s equation [44] (see **Materials and Methods**), we calculated that *ca.* 5 residues are in α-helical conformation.

The partitioning of membrane-active peptides into membrane interfaces favors formation of hydrogen bonds and acquisition of secondary structure [60]. No significant changes were observed in the CD spectra of 24.8 μM BP100 upon adition of POPC LUVs, at peptide:lipid ratios ranging from 1:1 to 1:40 (not shown). In contrast, considerable spectral changes took place in the presence of POPC:POPG LUVs, indicative of a more ordered structure. The positive band around 196 nm and the two negative bands, around 208 nm and in the 220–230 nm region (Fig. 2A, C, E, and G) showed that BP100 acquired α-helical conformation upon binding to POPC:POPG bilayers, pointing to the importance of electrostatic interactions for membrane binding, as noted by Ferre et al. [28].

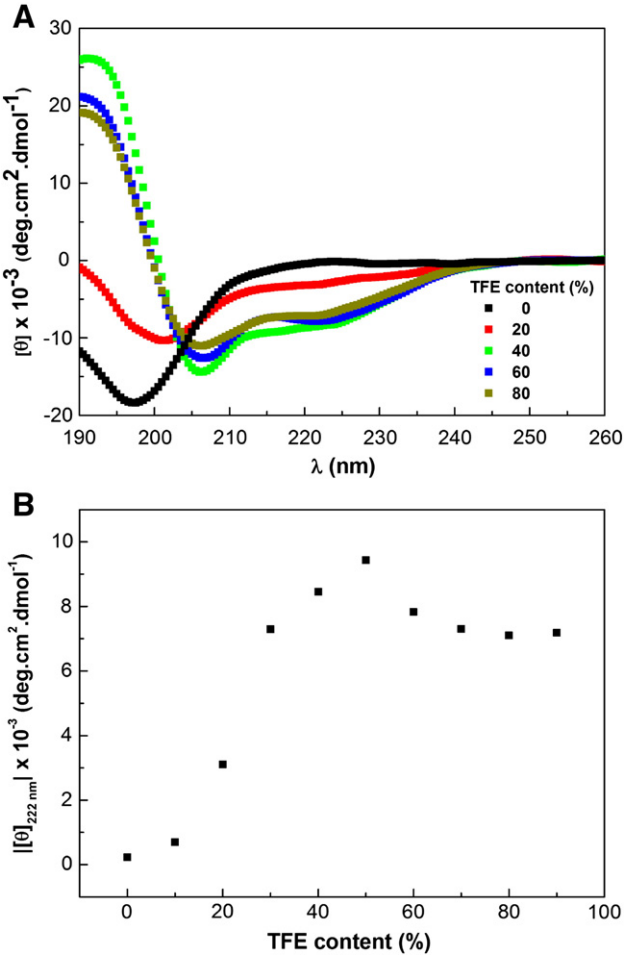

Fig. 1. Far-UV CD spectra of 27.4 μM BP100. **A**. TFE content (v %): 0 (■), 20 (■), 40 (■), 60 (■), and 80 (■); **B**. Modulus of [θ] at 222 nm as a function of TFE (v %).

Spectra were obtained as a function of lipid concentration for LUV containing the following POPC:POPG molar ratios: 75:25, 50:50, 25:75, and pure POPG (Fig. 2A, C, E, and G). CD spectra of membrane-bound BP100 for a limited range of lipid compositions and peptide:lipid molar ratios have been reported [27,32,33]. In general, a gradual increase of α-helical conformation was observed upon increasing lipid concentration (Fig. 2). The spectral features also varied with POPC:POPG molar ratios. Several spectra displayed features typical of membrane-bound peptides, namely, a shift to longer wavelengths and a decreased intensity of the band at 208 nm with respect to that in the 220–230 nm region. These features have been extensively related to differential absorption flattening and differential light scattering due to aggregates present in the sample [61–63]. Making use of Chen´s equation [43], we found that *ca.* 6 residues of BP100 are in α-helical conformation upon binding to POPC:POPG 50:50 bilayers, a number close to that obtained in 90% TFE (see above). This result is in agreement with the CD studies in ref. [34].

The panels on the right of Fig. 2 (Fig. 2B, D, F, and H) display the wavelengths at which minimum [θ] values ($[\theta]_{min}$) were observed in the 220–230 nm range ($\lambda_{\theta min}$), as well as the calculated charge of the (peptide + lipid) system assuming a + 6 charge for the peptide. For POPC:POPG molar ratios of 75:25 and 50:50 (Fig. 2A and C), $\lambda_{\theta min}$ red-shifted to a maximum wavelength in the region of electroneutrality of the system, decreasing thereafter. For POPC:POPG 25:75 and pure POPG (Fig. 2F and H), $\lambda_{\theta min}$ red-shifted to a maximum close to electroneutrality, but, in contrast to the former cases, this wavelength remained essentially constant even when the system's total charge was considerably negative.

3.1.2. NMR studies

To analyze the conformational properties of BP100 at greater molecular detail, we did NMR studies of the peptide in the presence of LUVs of PC and PC:PG by adding excess ligand (BP100). When the equilibrium between free and bound ligand is faster than the time necessary to build up NOEs (milliseconds), it is possible to obtain the NOEs of the bound state (as described in ref. [64]). These NOEs enabled structure determination of the bound peptide, without any prior knowledge of the structural features of the lipid bilayer. We have previously used this method to study peptide-membrane interaction [65,66].

BP100 resonances were sequentially assigned using the combination of TOCSY and ROESY spectra. Usually for small peptides, NOEs at the laboratory frames can be zero, while NOEs at the rotating frame, from ROESY experiments, give non-zero correlations. Sequential αN(i, i + 1) NOEs at the rotating frame were clear for many residues. When sequential NOEs were absent, the typical TOCSY pattern of each aminoacid residue was used. ^{13}C-HSQC and ^{15} N SOFAST-HMQC spectra were also acquired using natural abundance; this was important to overcome ^{1}H chemical shift overlaps. The backbone atoms of most residues, with the exception of K^1 and K^2 were assigned. A partial assignment is summarized in Table 1.

The one-dimensional ^{1}H spectrum of BP100 was obtained by pre-saturating water for 1.5 s, at different concentrations of BP100 and LUVs (Fig. 3A). Because of the lack of stable secondary structure of BP100, the peptide amidic hydrogens were saturated in the presence of PC LUVs. When the membranes contained PG, the amidic hydrogens were more protected from exchange with water and their NMR signal was less attenuated by water pre-saturation, indicating that these hydrogens were involved in hydrogen bonding. This is a strong indication of structure acquisition due to peptide binding to PC:PG LUVs, in agreement with CD data.

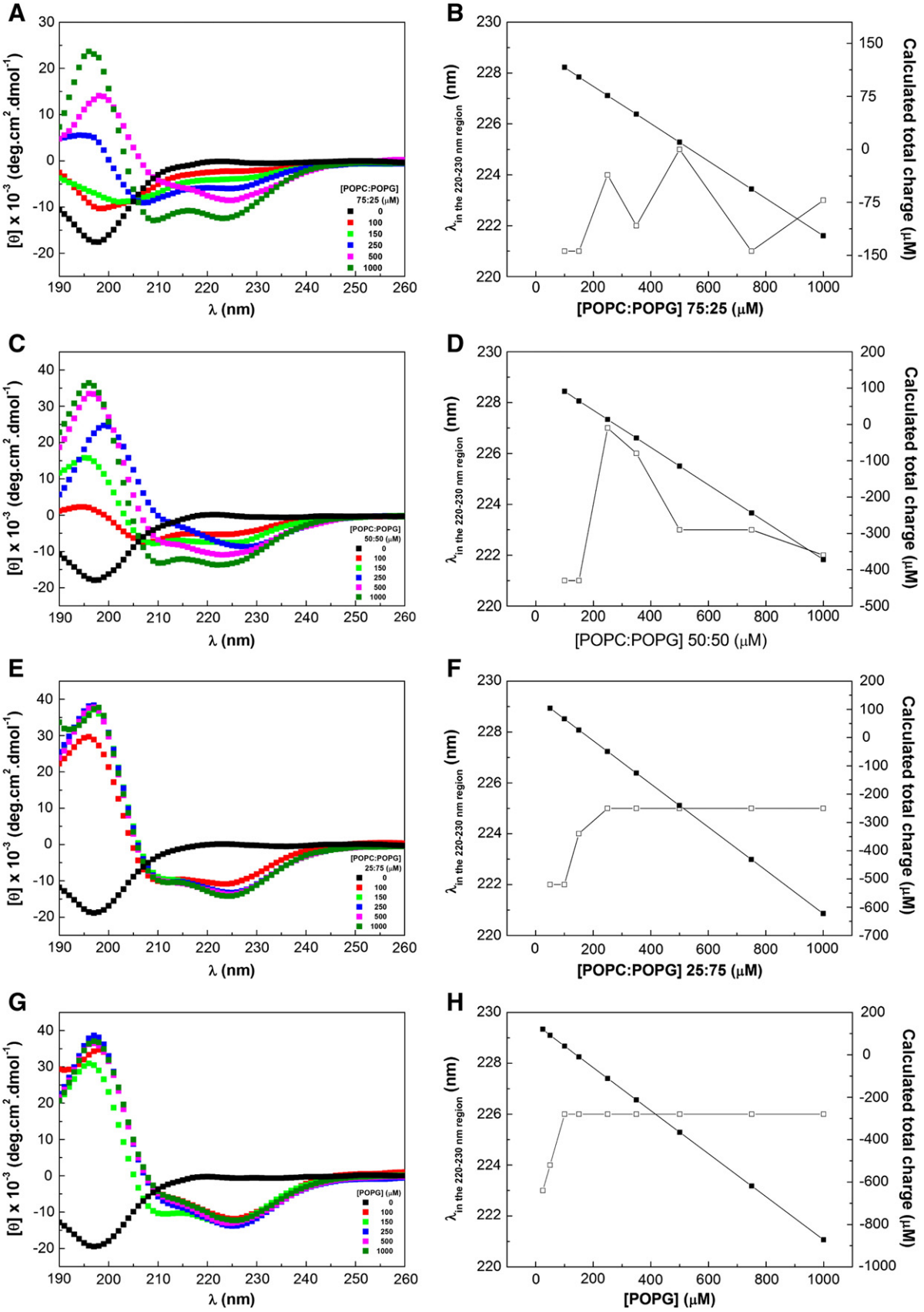

Fig. 2. Left: Far-UV CD spectra of 24.8 μM BP100 in the presence of increasing concentrations of POPC:POPG LUVs of variable composition. **A.** 75:25; **C.** 50:50; **E.** 25:75; **G.** pure POPG. Total lipid (μM): 0 (■); 100 (■); 150 (■); 250 (■); 500 (■); 1000 (■). The peptide:lipid molar ratios were 1:4, 1:6, 1:10, 1:20, and 1:40, respectively. Right: Wavelength (λ) of the negative peak in the 220–230 nm region (□) and calculated total charge of the peptide + lipid system (■), assuming total binding and a charge of +6 for the peptide.

Table 1
Partial Resonance Assignments of BP100 at 25 °C, pH 7.4. Values displayed in ppm and referenced as described by Wishart et al. [44].

	N	HN	Cα	Hα	Cβ	Hβ	Hγ	Cδ	Hδ
L^3	127.6	8.33		4.36	42.5	1.51		24.8	0.926
						1.60			
F^4	122.4	8.34		4.36	3 9.7	3.01			
						3.10			
K^5	124.6	8.32	54.7	4.38					
K^6	125.5	8.16	56.1	4.26					
I^7	123.8	8.26	60.8	4.15	38.5	1.85	1.18	12.6	0.864
L^8	127.6	8.33		4.36	42.5	1.51		23.5	0.859
						1.60			
K^9		8.27		4.25		1.73			
Y^{10}	121.7	8.20	57.7	4.58	42.0	3.00			
L^{11}	122.3	8.17		4.25	30.0	1.52		17.47	0.878
						1.59			

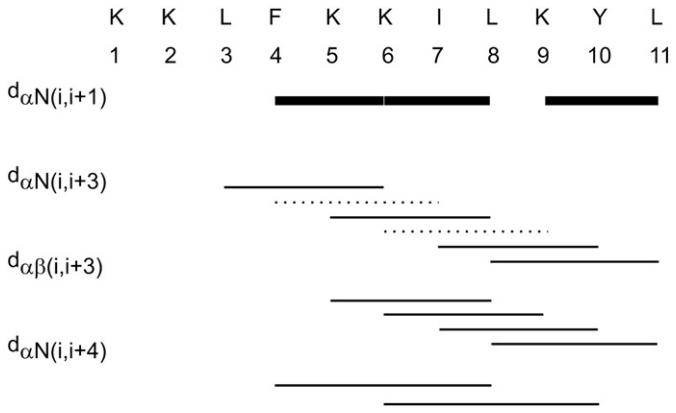

Fig. 4. Secondary structure plot. Summary of ambiguous transfer NOEs observed for BP100 in the presence of 90:10 PC:PG LUVs. Solid lines reflect strong and medium intensity NOEs and dashed lines indicate weak NOEs.

Transfer NOESY spectra in the presence of LUVs were also obtained (Fig. 3B). The spectra of BP100 in aqueous solution did not show NOEs at 100 ms mixing time; due to the high peptide flexibility, only very low intensity NOEs, indistinguishable from intraresidual ones, could be observed. A similar behavior was observed in the presence of pure PC LUVs, indicating that the peptide did not bind significantly to these vesicles. In the presence of PG-containing LUVs, a significant number of transfer NOEs was observed, again pointing to structure acquisition upon binding to these LUVs. This spectrum indicated the presence of NOEs typical of α-helical conformation for BP100 in the presence of 90:10 PC:PG LUVs (Fig. 4). The number of NOEs, as well as the intensity of the ^{1}H spectrum, decreased upon increasing the PG content from 90:10 to 70:30 PC:PG.

3.2. Effect of BP100 on the hydrodynamic diameter, D_h, and zeta potentials, ζ, of LUVs containing variable PC:PG molar ratios

The D_h´s of pure PC LUVs in 0.01 M Tris-HF, pH 8.1, did not vary upon addition of BP100 (Fig. 5). In contrast, strong effects were observed for PC:PG LUVs probably due to the electrostatic interaction between the positively (+6) charged peptide and negatively charged PG. The initial D_h of LUVs of variable PC:PG molar ratios was 95 ± 10 nm (Fig. 5), with a polydispersity index (PDI) < 0.1. The PDI remained < 0.1 with increasing BP100 concentration until electroneutrality, where both D_h (Fig. 5A) and PDI increased considerably, indicating vesicle aggregation, as suggested by the CD data (Fig. 2). It is noteworthy that between 3 μM and 6 μM BP100, the D_h of vesicles containing PG molar ratios of 30% and higher increased to *ca.* 140 nm (Fig. 5B), remaining approximately constant until electroneutrality.

For LUVs of pure PC, the initial values of ζ were, respectively, *ca.* -10 mV and −1 μm.cm/V.s (Fig. 6). Differential ion binding to zwitterionic phospholipids could be responsible for the small negative potential of the PC LUVs [67–70]. Addition of BP100 to 90:10 and 80:20 PC:PG LUVs caused a continuous decrease in the absolute values of ζ (Fig. 6A). Increasing the PG molar ratios produced extremely different results in the ζ *vs* BP100:lipid ratio patterns. A clear plateau,

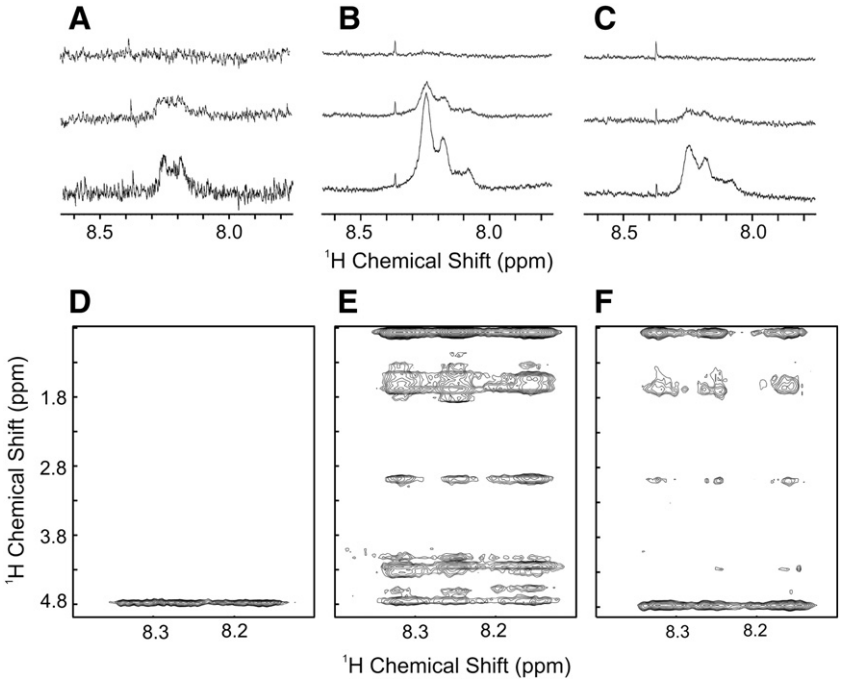

Fig. 3. NMR spectra of BP100 upon interaction with LUV. Amidic region of the one-dimensional ^{1}H-spectra (A, B and C) and 2D NOESY spectra (D, E and F) of BP100 in 15 mM Tris:HCl buffer, pH 7.4, 50 mM NaCl, in the presence of LUVs: Panels A and D show the results obtained with 5 mM PC; B and E show the results with 2 mM PC:PG 90:10 molar ratio; and C and F show the results obtained with 2 mM PC:PG 70:30 molar ratio. BP100 concentrations (μM) for the 1D spectra were 100 (top spectra), 400 (middle), and 800 (bottom). 2D experiments were acquired with 800 μM BP100 concentration. Note that transfer NOEs only appear when PG is present. The peak at 8.35 ppm in panels A, B, and C corresponds to a low molecular weight contaminant in the LUVs that appears in all spectra.

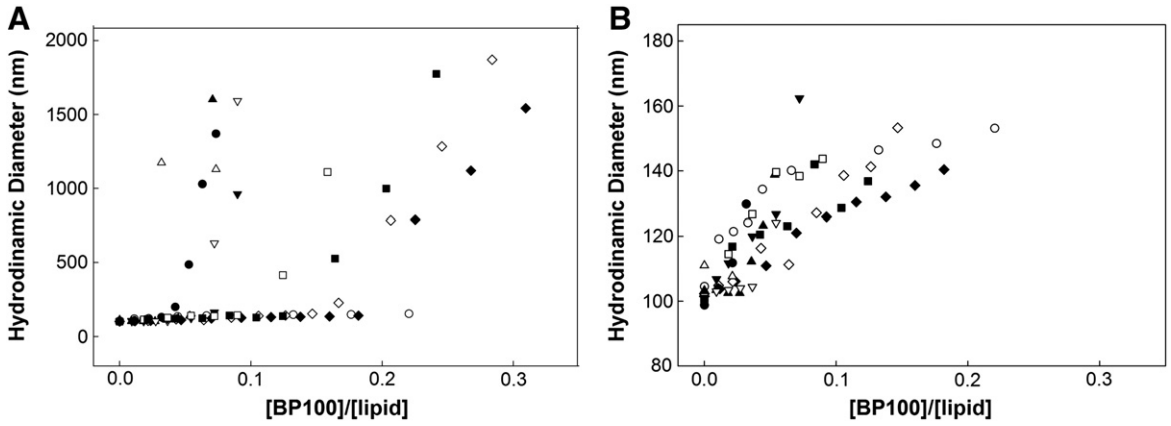

Fig. 5. D_h of LUVs at variable PC:PG molar ratios. Pure PC (○); 90:10 (●); 80:20 (△); 70:30 (▲); 60:40 (▽); 50:50 (▼); 30:70 (□) 20:80 (■); 10:90 (◇) pure PG (♦). Left: the ordinate scale ranges from 0 to 2,000 nm. Right: the ordinate scale ranges from 0 to 180 nm. Total lipid concentration, 125 μM, 10 mM Tris-HF buffer, pH 8.1.

where ζ did not vary as the BP100:lipid ratio increased, became more evident as the PG molar ratio increased (Fig. 6A and B). This behavior became much more pronounced for vesicles containing higher PG proportions. After reaching a plateau, where the value of ζ was independent of peptide: lipid molar ratio, further increasing this ratio produced a sharp decrease in the absolute value of ζ. The BP100:lipid ratio where this sharp increase of ζ occurred varied as a function of PC:PG molar ratio (Fig. 6A and B). In general, values of ζ near zero were obtained at PG concentrations approximately six times that of BP100, as observed by Freire et al. [71]. In the region close to ζ ≅ 0 there is high data dispersity probably due to BP100-induced aggregation of LUVs.

3.3. BP100-induced leakage of LUVs containing variable PC:PG molar ratios

We investigated the peptide effect on the leakage of fluorescent probes incorporated in the inner aqueous compartment of LUVs. The conformational studies (**Section** *3.1*) and the measurements of hydrodynamic diameter and of ζ (**Section** *3.2*) provided clear evidence for the importance of electrostatic interactions on peptide binding. Therefore, we examined the effect of ionic strength on BP100-induced leakage.

For studies at low salt (20 mM Tris–HCl, pH 8.1), leakage was monitored using the PTS/MV system (see **Section** *2.2*). The effect of BP100 concentration on PTS leakage was studied with LUVs prepared at several PC:PG molar ratios as a function of time.

In the absence of BP100, LUVs of pure PC containing PTS were stable and the PTS leakage after 15 min was *ca.* 3 % (not shown). Fig. 7A presents the effect of varying BP100 concentration on PTS leakage from LUVs containing PC:PG 50:50 as a function of time, at a fixed LUV concentration. With PC:PG 50:50 LUVs, without BP100, the PTS leakage after 15 min was *ca.* 12 %, showing that vesicles containing negatively charged PG were more leaky, possibly due to charge repulsion between phospholipids (Fig. 7A, line a). It is likely that MV outside the LUVs containing PTS also contributes to vesicle destabilization due to binding of the MV di-cation to PG. BP100 addition to 50:50 PC:PG LUVs caused a peptide concentration-dependent decrease in PTS fluorescence (Fig. 7A).

In the presence of BP100, the kinetics of PTS leakage (Fig. 7A) were more complex at the lower peptide:lipid molar ratios; the shapes of the curves were different with increasing BP100 (compare, for example, curves c and f in Fig. 7A) suggesting changes in mechanism and/or rate limiting steps of leakage.

The extent of peptide-induced leakage as a function of BP100:lipid ratios with LUVs at several PC:PG molar ratios was compared by analyzing the percentage of leakage at a fixed time (850 s) and LUV concentration (Fig. 7B). As an example, the % leakage for each BP100 concentration, at 850 s, with PC:PG 50:50 LUVs (Fig. 7A), was calculated and plotted *vs* BP100:lipid molar ratio (Fig. 7B). Each line in Fig. 7B corresponds to LUVs of different PG:PG molar ratios and was constructed from sets of data similar of those in Fig. 7A. Clearly, the BP100 concentration required for 50% leakage decreased with increasing PG content in LUVs (Fig. 7B).

In order to clarify the influence of the PG content on LUVs permeability, the percentage of PTS leakage, at a fixed BP100:lipid molar

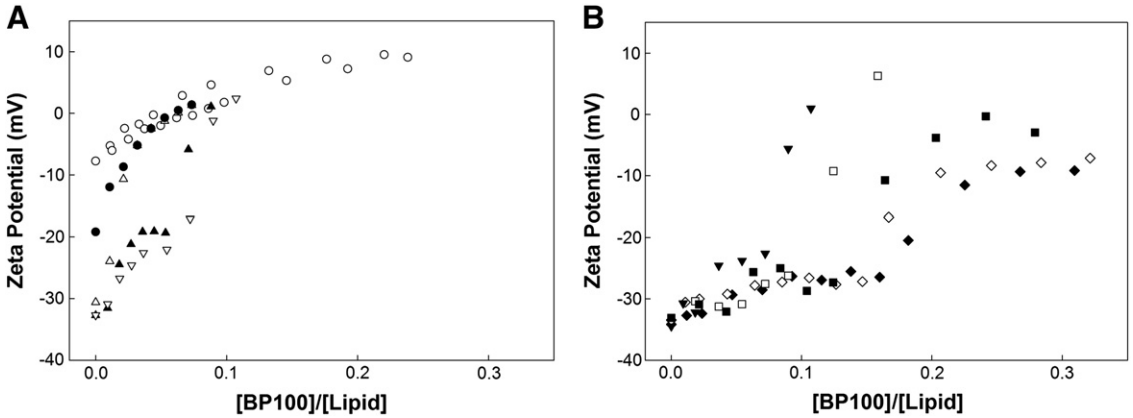

Fig. 6. Zeta potential as a function of BP100 concentration for LUVs with variable PC:PG molar ratio. **A**. Pure PC (○); 90:10 (●); 80:20 (△); 70:30 (▲); 60:40 (▽). **B.** PC:PG molar ratio 50:50 (▼); 30:70 (□); 20:80 (■); 10:90 (◇); pure PG (♦). Total lipid concentration: 125 μM, 10 mM Tris-HF buffer, pH 8.1.

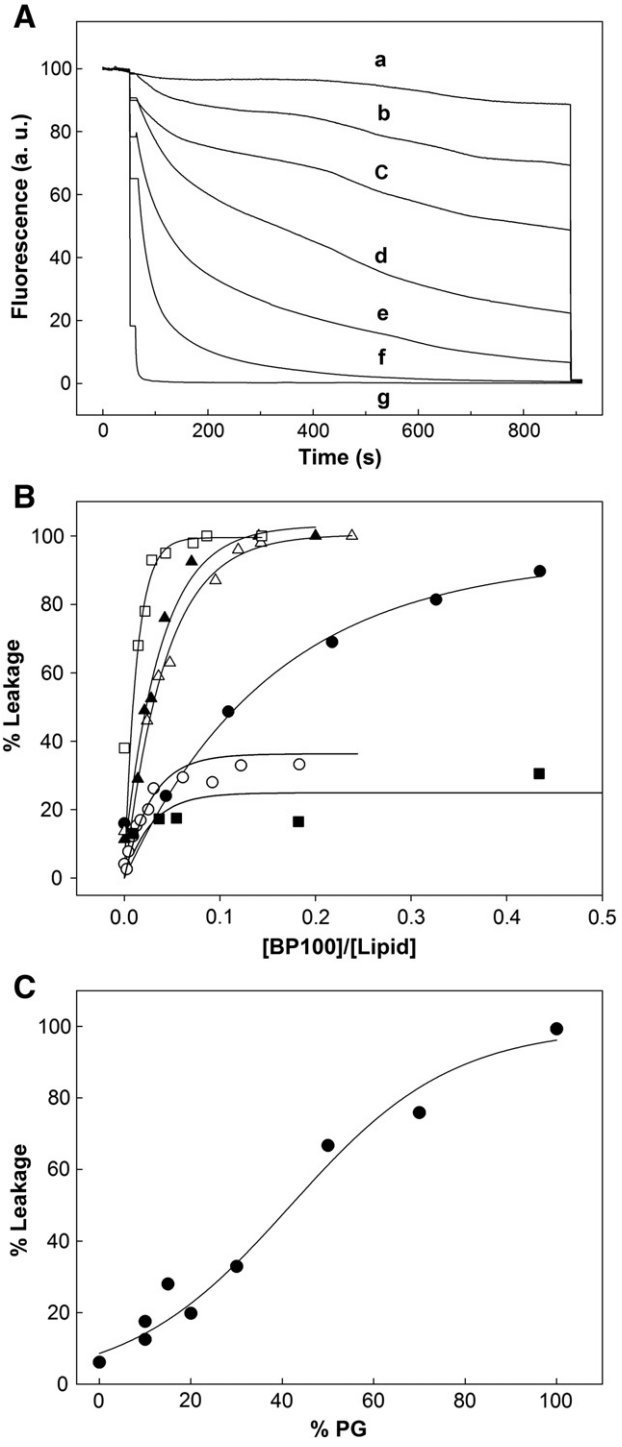

Fig. 7. A. PTS leakage from LUVs upon addition of BP100 at low ionic strength. A. Leakage of PTS from 50:50 PC:PG LUV as a function of time for increasing BP100 concentration (μM): a) zero; b) 0.25; c) 0.50; d) 0.75; e) 1.25; f) 1.42; g) 2.50. **B.** Effect of peptide:lipid molar ratio on PTS leakage, after 850 s. PC:PG 90:10 (○); PC:PG 85:15 (●); PC:PG 70:30 (△); PC:PG 50:50 (▲); PC:PG 30:70 (□); pure PG (■). **C.** PTS leakage as a function of PG content at BP100:lipid molar ratio of 0.08, at 850 s. Total lipid concentration, 17.8 μM, 14 mM Tris–HCl, pH 8.1, MV concentration, 1 mM.

ratio (0.08), time (850 s) and LUV concentration, was plotted vs % PG (Fig. 7C). As can be observed in Fig. 7C, the percentage of PTS leakage increased sigmoidally with increasing PG content.

To analyze the effect of higher ionic strength on BP100-induced leakage, LUVs were loaded with 50 mM CF and the external buffer contained 10 mM Tris–HCl, pH 8.1, and 300 mM NaCl (see **Section** 2.2). Addition of BP100 to LUVs at this salt concentration did not lead to vesicle aggregation, in contrast to the experiments performed at low ionic strength, where aggregation was observed in some samples.

LUVs of pure PC were very stable at high ionic strength; after *ca.* 30 min, only 1.5% leakage was detected (not shown). Addition of 2.5 μM BP100 to PC LUVs induced *ca.* 15% leakage after 40 min, indicating a small BP100 effect (not shown). Fig. 8A shows the time course of CF leakage from a fixed concentration of 50:50 PC:PG LUVs as a function of BP100 concentration. Although the leakage rates were slower at higher ionic strength, the kinetic profiles were similar to those obtained

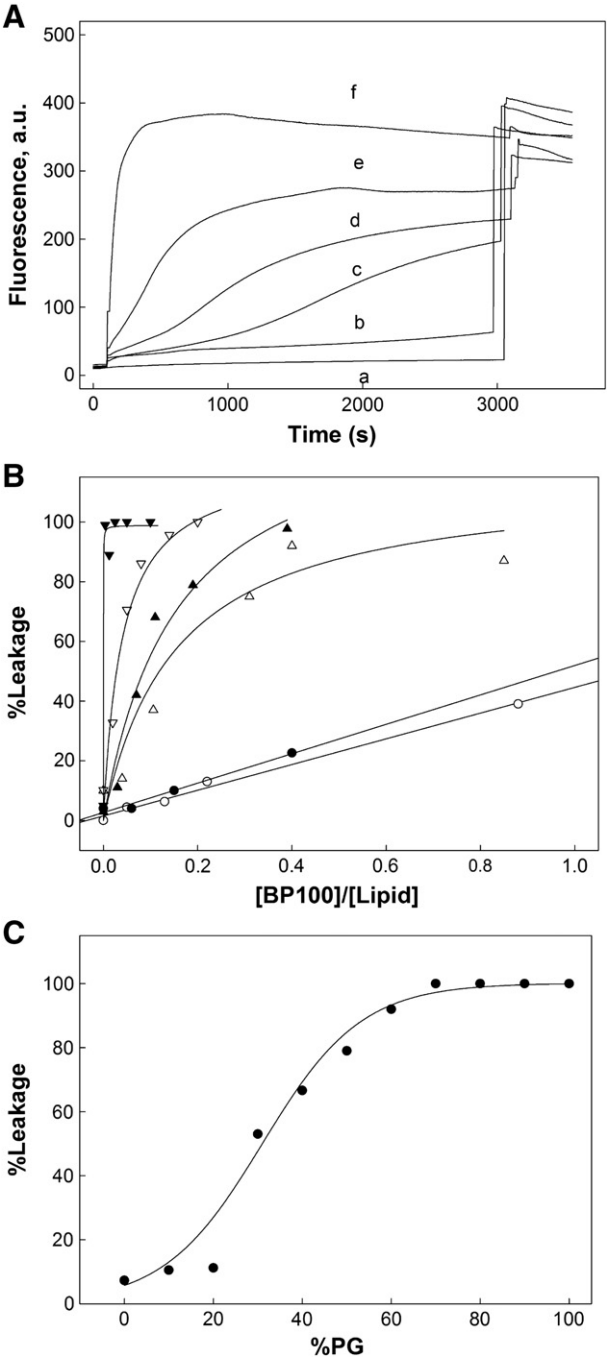

Fig. 8. CF leakage from LUVs upon addition of BP100. A. Leakage from 50:50 PC:PG LUV as a function of time for increasing BP100 concentration (μM): a) zero; b) 0.84; c) 1.26; d) 1.98; e) 3.42; f) 6.84. **B.** Effect of peptide:lipid molar ratio on leakage, after 2,400 s. PC:PG 90:10 (○); 80:20 (●); 70:30 (△); PC:PG 50:50 (▲); PC:PG 30:70 (▽); pure PG (▼). **C.** Leakage of CF as a function of PG content at a BP100:lipid molar ratio of 0.2 after 2,400 s. Lipid concentration, 18 μM, 10 mM Tris–HCl buffer, pH 8.1, 300 mM NaCl.

at low ionic strength (Fig. 7A). The kinetics were also more complex at the lower peptide:lipid molar ratios (*e.g.*, compare curves c and f in Fig. 8A).

The effect of BP100:lipid ratios and PG content was compared at 2400 s, at the same LUV concentration (Fig. 8B). Each curve in Fig. 8B corresponds to different PC:PG molar ratios and was obtained from a set of experiments similar to those in Fig. 8A. The BP100 concentration required for 50% leakage also decreased with increasing PG content (Fig. 8B). The CF leakage as a function of PG content at a 0.2 BP100:lipid ratio, time (2,400 s), and LUV concentration is shown in Fig. 8C; clearly, as seen at low ionic strength (Fig. 7C), leakage also increased sigmoidally with increasing negative charge.

The effect of ionic strength on LUVs leakage was evaluated by comparing the leakage of LUVs of PC:PG 50:50 at a fixed time (800 s) and very similar total lipid concentration (17.8 μM and 18 μM, Fig. 9) as a function of BP100:lipid molar ratio. Increasing the BP100:lipid molar ratio increased leakage at both low and high ionic strength. However, the BP100:lipid molar ratios producing 50% leakage were very different, *i.e.*, 0.023 at low and 0.16 at high ionic strength. Fifty percent leakage required ca. 7 times more BP100 at the higher ionic strength.

3.4. Optical microscopy of GUVs in the presence of BP100

The effects of BP100 on GUVs of POPC or POPC:POPG (70:30 molar ratio) were examined using phase contrast optical microscopy. GUVs in the absence of peptide were stable under the microscope and retained the sugar asymmetry for, at least, four hours of observation, which is the time scale of the experiments. An aliquot of a GUV suspension was added to an observation chamber containing a 50 μM BP100 solution and individual GUVs were selected and followed with time. The peptide effect on GUVs of POPC:POPG (Fig. 10A) and POPC (Fig. 10B) was dependent on membrane charge. POPG-containing GUVs were observed to burst in the presence of peptide, as shown for two GUVs in Fig. 10A (at 551 s and 570 s). Bursting was characterized by a fast (within less than a second) collapse of the GUV into dense peptide-lipid aggregates (see last snapshot at 570 s). Several dense patches (indicated with arrows in Fig. 10A) were often observed on the surface of both vesicles before the final bursting event. The formation of these dense regions is also induced by other antimicrobial peptides, such as gomesin [53] and MPX [72], and has been interpreted as arising from a local membrane bending mediated by the peptides, which would act as linkers between apposed layers. Therefore, these regions, which are similar to the remains after vesicle burst, indicate a dense peptide-lipid aggregate. The occurrence of this phenomenon could be analogous to BP100-induced vesicle aggregation observed with LUVs (see Fig. 5).

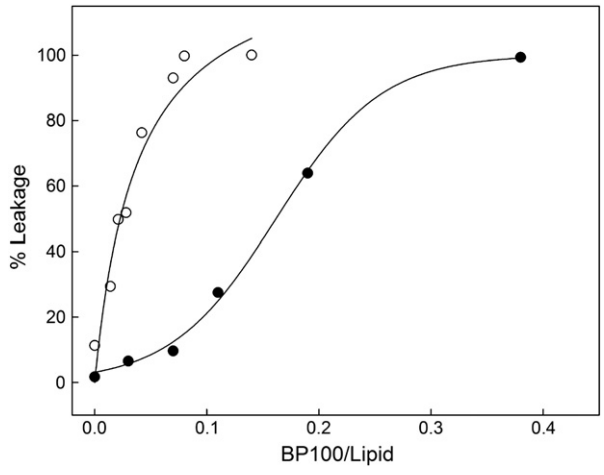

Fig. 9. Effect of BP100:Lipid ratio on the leakage of CF and PTS. (●) CF in 10 mM Tris–HCl buffer, pH 8.1, 300 mM NaCl and (○) PTS in 14 mM Tris–HCl, pH 8.1, and 1 mM MV. The membrane consisted of 50:50 PC:PG and the total lipid concentration was 17.8 and 18 μM for LUVs with PTS and CF, respectivelly. All data were obtained after 800 s.

Different effects were observed for GUVs of pure POPC. Even though some GUVs burst in a manner similar to that seen in Fig. 10A, many vesicles remained intact but lost their optical contrast, conferred by the original sucrose/glucose asymmetry. Fig. 10B shows one such example. Dense patches were also observed on the surface of the GUVs (see arrows in Fig. 10B). After 440 s, the GUV began to lose its optical contrast, which was completely lost after 540 s. Even after long contact times with the peptide solution (15 min), many GUVs were still stable, although without the original optical contrast. These results indicate that BP100 is able to permeabilize POPC GUVs without disrupting the vesicle. It should be noted that high peptide concentrations and low lipid concentrations were used in this study. Moreover, although no acquisition of secondary structure was detected by CD or NMR, the peptide did have a small effect on the zeta potential (Fig. 6) and leakage (Fig. 7) of PC LUVs, both at low (not shown) and high (Fig. 8B) ionic strength. These results are in accordance with the effects observed in pure POPC GUV.

4. Discussion

We examined the conformational properties of BP100 in the absence and presence of model membranes using theoretical approaches, as well as CD and NMR spectroscopy. The effect of BP100 upon structural and functional properties of the membranes was investigated by measuring hydrodynamic diameter, zeta potential, and leakage of LUVs inner contents at low and high ionic strength. The peptide-membrane interaction was also monitored by means of optical microscopy of giant unilamellar vesicles (GUVs). This multiple approach provided a detailed picture of the events taking place upon the salt-dependent BP100-bilayer interaction and demonstrated that the peptide´s mechanism of action depends on peptide:lipid ratio and membrane surface charge.

4.1. Conformational properties of BP100

Theoretical prediction [54] and calculation of the mean hydrophobicity and mean hydrophobic moment according to Eisenberg et al. [56] revealed that the peptide displays a propensity to fold as a surface-seeking amphipathic α-helix, with a polar angle of 180°, as shown by OCD and solid state NMR studies [34]. Interestingly, the helix polar surface consists of five lysine residues, K^1, K^2, K^5, K^6, and K^9 (Scheme 1), giving rise to a curved surface with a 1.2 nm length covered by five positive charges, plus the N-terminus, allowing the interaction with negative charges on the membrane surface.

CD and NMR spectra showed that, upon binding to LUV containing negatively charged PG, BP100 acquired α-helical conformation. Peptide binding to zwitterionic PC membranes was not detected by CD or NMR, emphasizing the importance of electrostatic interactions for BP100-membrane interaction. It should be noted, however, that small effects of BP100 were observed in the studies of zeta potential (Fig. 6) and vesicle leakage (Figs. 7 and 8). Moreover, BP100 exerted an effect on GUV of pure PC (Fig. 10). Since it has been extensively shown both experimentally [67–70] and by molecular dynamics [73] that zwitterionic PC bind ions, it is conceivable that BP100 binds to pure PC LUVs to a small extent, not enough to allow the detection by CD or and NMR . In addition, weak binding may be related to a shallower peptide location, not sufficient to promote achievement of secondary structure.

When LUVs contained negatively charged PG, BP100's CD spectral features depended on both peptide:lipid ratio and PG content. For POPC:POPG molar ratios of 75:25 and 50:50 (Fig. 2A and C), the wavelength of $[\theta]_{min}$ was red-shifted to a maximum, decreasing thereafter. It is noteworthy that this maximum occurred in the region close

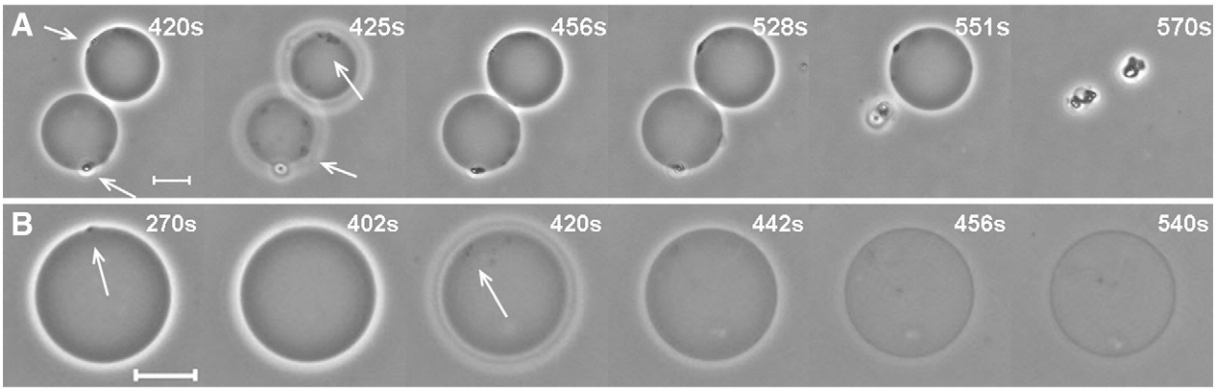

Fig. 10. Phase contrast optical microscopy of GUVs in the presence of 50 μM BP100. A. POPC:POPG (70:30, molar ratio); **B**. Pure POPC. The time on top of each snapshot refers to the time elapsed after addition of an aliquot of GUVs to the observation chamber filled with 50 μM peptide solution. The arrows indicate dense spots formed on the surface of the GUVs. The scale bars represent 10 μm.

to the system's electroneutrality. For POPC:POPG 25:75 and pure POPG (Fig. 2E and G), the wavelengths of $[\theta]_{min}$ were also red-shifted to a maximum wavelength when the system's charge was close to electroneutrality, but, in these cases, these values remained essentially constant even when the system's total charge was considerably negative.

The red shifts were probably due to peptide-induced vesicle aggregation, a condition favored by electroneutrality. For the lower PG contents, the red shift tended to disappear with increasing total lipid content, which leads to an increase of the system's total (negative) charge, suggesting that charge repulsion reversed aggregation. Vesicle aggregation under conditions close to electroneutrality was confirmed by quasielastic light scattering (**Section** 4.2). However, the fact that the wavelengths of $[\theta]_{min}$ remained red-shifted with increasing vesicle concentration suggested that aggregation persisted even at high lipid: peptide ratios for membranes containing high PG proportions. Since it does not seem realistic that vesicle aggregation would persist under conditions where the system's total charge becomes considerably negative (Fig. 2B, D, F, and G), it is conceivable that at these high PG molar ratios the peptide is capable of promoting lipid clustering, giving rise to areas of high peptide density. In these latter cases peptide aggregation on the membrane surface would be responsible for the observed red shifts of $[\theta]_{min}$. Subsequently, peptide-rich patches might be able to leave the bilayer, causing membrane disruption, which would explain the irreversibility of $[\theta]_{min}$ red shifts. As discussed below, this rationalization was validated by the results obtained in leakage experiments (**Section** 4.3) and in studies with GUV (**Section** 4.4).

Further analysis of the CD spectra also substantiates the notion of vesicle disruption for membranes with high PG content. An examination of Fig. 2 left panels (Fig. 2A, C, E, and G) reveals that in several spectra the negative band at *ca.* 208 nm becomes less intense than the band in the 220–230 nm region. This behavior, which is also an indication of aggregation, parallels the red shifts depicted in the right panels of the figure. As discussed above, it seems unlikely that the asymmetry in intensity of the two peaks would be due to vesicle aggregation remaining under conditions of considerable negative charge of the (peptide + lipid) system (Fig. 2B, D, F, and G). These spectral features observed for 25:75 POPC:POPG and pure PG represent additional evidence for peptide aggregation on the membrane surface, as well as peptide-induced lipid clustering. Membrane disruption could follow, giving rise to peptide-rich membrane fragments. Similar events have been described for the parent peptides melittin [74], cecropin [75], and for other hybrids of these peptides [23].

The leakage studies showed that, while peptide-induced leakage was relatively slow for vesicles of lower PG content, at all peptide:lipid ratios, leakage was, in our time-scale, essentially instantaneous in the case of vesicles with higher PG content, especially at the higher peptide:lipid ratios. Thus, the features observed in the CD spectra (red shifts and lesser intensity of the peak centered at *ca.* 208 nm) for samples with higher PG contents would be due either to peptide high concentration in clusters, giving rise to highly leaky vesicles, or to vesicle disruption, or both phenomena occurring sequentially. On the other hand, lipid clustering would not occur in membranes with lower PG content, or would occur to a low extent, in a time-dependent process. Although the experiments were not performed under similar conditions, vesicle disruption and formation of peptide-lipid dense regions were observed with GUVs (**Section** 4.4).

BP100-promoted lipid clustering was not detected in calorimetric experiments with phosphatidylethanolamine (PE):cardiolipin membranes at 75:25 molar ratio [33]. Although this lipid composition is different from those used in the present study, the results of Wadhwani et al. [33] agree with the present data that suggest that clustering does not occur to a significant extent in membranes with lower PG contents.

As for the NMR data, transfer NOEs can be used to calculate the structure of bound BP100. However, we decided not to conduct direct structural calculations for BP100 in the presence of PC:PG LUVs since the resonances were highly ovelapped in the transfer NOESY spectra and the NOEs were ambiguous. Nevertheless, since CD indicated that a helical structure was stabilized in the presence of PC:PG LUVs (Fig. 2), we made use of these data to analyze the NMR data. Thus, we decided to look for answers to two important questions: (i) what type of helix is stabilized? (ii) which residues are involved in helix formation? An examination of the transfer NOESY spectrum indicated the presence of NOEs typical of α-helical conformation for BP100 in the presence of 90:10 PC:PG LUVs (Fig. 4). NOEs for an α-helix spanning residues L^3 to L^{11} were deduced together with αN(i, i + 3) and αβ(i, i + 3) for all residues in this region and two αN(i, i + 4) that are present only for α-helices. Residues K^1 and K^2 were not assigned. This analysis yields a higher α-helical content than that calculated from the CD spectra. Very likely, this difference is influenced by the effect of vesicle aggregation on the CD spectra. Moreover, according to Manning et al. [76], the minimum helix length required to produce an α-helix-like CD spectrum is two to three turns (seven to eleven residues). It is conceivable that BP100 is not sufficiently long to yield CD spectra corresponding to the actual helix length.

The number of NOEs, as well as the intensity of the ^{1}H spectrum, decreased upon increasing the PG content from 90:10 to 70:30 PC:PG, indicating an increase in binding affinity with increasing PG content. At 70:30 PC:PG molar ratio, conditions for transfer NOE were not ideal because of the increase in binding affinity and consequent slower exchange regime. The decrease in signal intensity is attributable to broader ^{1}H lines. Increased peptide binding with increasing PG content is in agreement with the leakage studies (**Section** 4.3).

4.2. Effect of BP100 on particle size and surface electrical properties

Quasielastic light scattering data showed that, while the hydrodynamic diameter (D_h) of PC LUVs was essentially constant in the presence of BP100, addition of the peptide to PG-containing LUVs at low ionic strength caused significant effects on D_h (Fig. 5A). At higher peptide concentrations, and for all PG contents, D_h and PDI increased considerably, indicating vesicle aggregation, as suggested by the CD data (Fig. 2).

The results obtained for zeta potential measurements (Fig. 6) can be rationalized by assuming that in LUVs containing less than 30 mole % PG, the phospholipid negative charges are well separated and only a small fraction of buffer ions bind to the membrane surface. In fact, the limit of *ca.* 30% surface charge necessary for ion condensation and stability of charged particles with little electrostatic repulsion at the interface is well known [77,78]. Addition of the peptide leads to charge neutralization with a continuous decrease in ζ.

The data in Fig. 6B clearly show that, although the peptide does bind to the LUVs upon addition of the initial BP100 aliquots, the zeta potential of the vesicles in this region remains constant. The most likely and simplest explanation for this observation considers that the stability of several aggregated systems depends on a constant surface potential. In order to maintain a constant surface potential, binding of positively charged molecules has to be compensated by displacement of counterions bound to the negatively charged headgroups. Our data do not allow a distinction between the enthalpic (coulombic) and entropic components that determine the stability of the aggregated system with constant surface potential and the measurement of zeta potential cannot inform on hydrophobic binding.

For LUVs containing >30 mole % PG, the average distance between the PG molecules decreases, and repulsion increases, potentially decreasing vesicle stability, particularly at low ionic strength. Charge repulsion, due to proximity of like-charged groups at the interface in vesicles and other amphiphilic aggregates, decreases by counterion condensation leading to lower free energy and aggregate stabilization [79]. In PG-containing LUV, condensation of Na^+ and $TrisH^+$ counterions at the surface contribute to vesicle stabilization by neutralizing part of the negative charge [80]. The positively charged BP100 can ion-exchange, displacing bound cations and maintaining the total vesicle charge [81]. Ion exchange is the most plausible explanation for the regions of Fig. 6 where the ζ essentially does not vary with increasing BP100:lipid ratio. It is noteworthy that in the region between approximately 3 μM and 6 μM BP100, the size of vesicles, containing PG molar ratios of 30% and higher, increased to *ca.* 140 nm (Fig. 5B), and remained approximately constant until electroneutrality, suggesting that peptide binding at low BP100:lipid ratios promotes an increase in vesicle size. This behavior suggests that the vesicle charge only changes appreciably after interfacially bound counterions are exchanged for BP100. The residual negative vesicle charge can then be completely neutralized by further peptide addition. At this point, the values of electrophoretic mobility do not reflect the mobility of isolated vesicles due to vesicle aggregation (Fig. 5A).

The fact that electroneutrality was achieved at a *ca.* 1:6 BP100:PG molar ratio strongly suggests that both the outer and inner bilayer leaflets are accessible to the peptide. In fact, it was reported that BP100 can translocate across model membranes [28]. In addition, experiments with GUVs (**Section** 4.4) showed that membrane disruption can occur in the presence of BP100. Although experiments with GUVs have not been performed in conditions similar to those of ζ measurements, the possibility of membrane disruption in the latter experiments should also be considered, especially at the higher PG contents and high peptide:lipid ratios. Disruption of *E. coli* cell envelope was reported by Alves and coworkers [26].

4.3. Effect of BP100 on leakage of vesicle inner contents

Since the interaction between positively charged peptides and the lipid components of membranes is strongly determined by electrostatic interactions, and since physiological media contain several charged species, we found it important to examine the effect of ionic strength on BP100-membrane interaction. Studies with PG-containing LUVs were performed at low (Fig. 7) and high (Fig. 8) ionic strength. The leakage kinetics depended on peptide:lipid molar ratio, being were complex at lower peptide:lipid molar ratios. The shapes of the kinetic curves are distinctly different with increasing BP100, suggesting possible changes in mechanism [82].

A quantitave comparison between the data at low and high ionic strength is not straightforward. However, an analysis of the data at fixed times provided an estimate of maximum ionic strength effects. Fig. 9 shows that, at BP100:lipid, addition of 0.3 M salt decreased the efficiency of the leakage processes seven fold. Ben-Tal and coworkers [83] also found an ionic strength dependence of the binding of pentalysine to membranes containing negatively charged phospholipids.

In view of the several events occurring upon BP100 interaction with charged vesicles, the determination of an ion exchange constant would be more appropriate to analyze this interaction at high ionic strength. Nevertheless, at low ionic strength an ion exchange constant as well as a binding constant can be used to characterize the system in conditions of minimum screening of electrostatic interactions [84].

The calculated total charges (in μM) of the (peptide + PG) systems in Fig. 7A are: −7.5, −6.8, −6.0, −4.5, −1.5, −0.5, and +6.0 (for curves a-g). Thus, the change in kinetic behavior takes place as the system approaches electroneutrality. Furthermore, as the PG content increased, the BP100 concentration required to reach 50% leakage decreased. Assuming the vesicle radius to be 50 nm, and the lipid cross section as 0.7 nm^2, we estimated the number of lipid molecules per vesicle to be approximately 86,000. For the data in Fig. 7B, we estimate that, in order to obtain 50% leakage, approximately 1.1 x 10^4 BP100 molecules are required per vesicle of PC:PG 70:30, whereas *ca.* 3,000 are required per vesicle of PC:PG 50:50, 2,000 per vesicle of PC:PG 30:70, and 900 per vesicle of pure PG. This suggests that the process is of cooperative nature, being strongly favored by increasing the membrane PG content. The cooperativity of the process is corroborated by the data in Figs. 7C and 8C, where the percentage of leakage is presented as a function of PG content. These results are in agreement with the findings of Mosior and MacLaughlin [85] and Ben-Tal et al. [83] who also found that the binding of pentalysine to membranes containing negatively charged phospholipids is of cooperative nature.

An additional remark concerns the fact that, although the interaction between BP100 and negatively charged membranes decreases at high ionic strength, binding still occurs to a considerable extent, indicating that other forces also contribute to binding. The hydrophobic nature of the residues in the apolar face of the amphipathic α-helix formed by BP100 (Scheme 1) very likely plays an important role in the hydrophobic contribution for peptide binding.

4.4. Effect of BP100 on GUV

The optical microscopy observations of GUVs agreed with the results obtained for LUVs, indicating that the effects of BP100 on membranes were modulated by surface charge. While BP100 induced bursting of negatively charged GUVs, membrane permeabilization without vesicle disruption was observed with PC GUVs (Fig. 10). Although the experimental conditions employed with GUVs are different from those used in experiments with LUVs (the peptide:lipid molar ratio is much higher and the lipid concentration is much lower), small effects were observed on ζ (Fig. 6) and on the extent of leakage of pure PC LUV upon addition of BP100. Nevertheless, no acquisition of conformation was detected in the presence of these membranes by CD and NMR (**Section** 4.1).

4.5. Mechanism of action of BP100

In spite of the wealth of literature on AMP-membrane interaction attempting to understand the mechanism of action of AMPs, a relatively

small number of studies points to the fact that this mechanism depends on conditions such as peptide:lipid ratio, as well as membrane lipid composition. The effects of these conditions on the mode of peptide binding, activity, and lipid organization have been reported both in experimental studies [*e.g.*, refs. 11–13,23,86,87] and molecular dynamics calculations [88–93] of AMP-membrane interaction.

The present results, as well as the above discussion, are consistent with the dependence of the mechanism of action of BP100 on peptide: lipid ratio and on the proportion of PG in the membrane. CD and NMR spectra provided evidence for α-helical conformation of membrane-bound BP100. Furthermore, OCD and solid state ^{15}N NMR data [34], as well as analysis by the Eisenberg formalism [56], indicated that BP100 is located on the membrane surface, with the helix axis parallel to the surface. In addition, the analysis of peptide location according to Eisenberg [56], indicated that BP100 is a surface-seeking peptide. Moreover, BP100 is too short to span the bilayer thickness, especially in the α-helical conformation. These aspects have to be taken into consideration when discussing the possible mechanism(s) by which the peptide affects membrane permeability.

Scheme 2 depicts the series of events proposed to occur under the different conditions examined in the present study. At low peptide: lipid ratios and low PG content the data do not provide evidence for either peptide and/or lipid aggregation. Moreover, the leakage data are indicative of a gradual loss of the contents of the vesicles inner aqueous compartment. This process could be due to peptide-promoted perturbation of the bilayer acyl chain organization caused by electrostatic interaction between the lipid and one or a few peptide monomers. It has been extensively shown that binding of small monomeric molecules mediated by different types of forces can affect acyl chain packing and, therefore, influence bilayer permeability. Different studies report either a decrease or an increase in acyl chain packing upon binding of positively charged peptides [94–97]. Moreover, other events may take place at low peptide:lipid ratios and low PG content, such as lipid clustering [18–20,98,99] which would promote formation of membrane defects at the border between peptide-bound and peptide-free clusters, and membrane thinning [100]. These phenomena could occur independently or concomitantly, leading to a gradual release of membrane inner contents. While the gradual release of inner contents is a consequence of membrane perturbation by a small number of peptide molecules (monomers or small aggregates), the essentially instantaneous loss of the inner contents, under conditions of high peptide:lipid ratio and high PG, would result from membrane disruption, the final step of a sequence of events – peptide-promoted lipid clustering, which in turn will promote peptide aggregation on the membrane surface, giving rise to peptide-lipid patches that eventually would leave the membrane in a carpet-like mechanism.

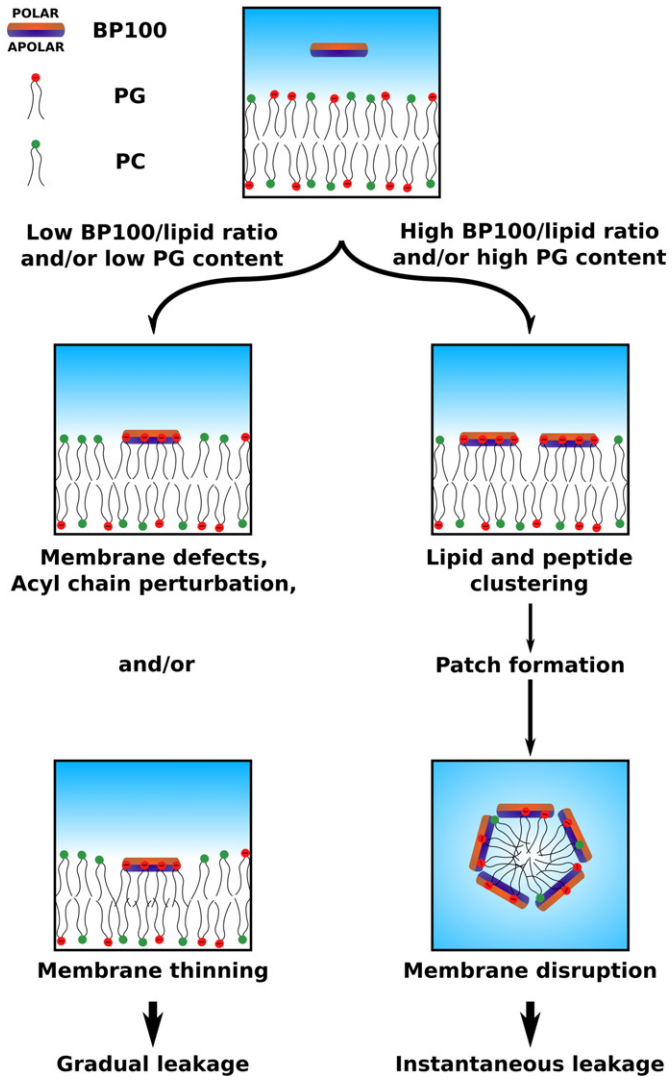

Scheme 2. Proposed events occurring at low (high) BP100/lipid ratios and low (high) PG contents. In the former (latter) case gradual (instantaneous) release of membrane inner contents would be observed.

Acknowledgements

The following funding agencies are acknowledged: FAPESP (2007/50970-5 and 2013/08166-5); CNPq, Instituto Nacional de Ciência e Tecnologia de fluidos complexos (INCTFCx), Núcleo de Apoio à Pesquisa de Fluidos Complexos (NAPFCx). We thank Drs. P. Di Mascio and F.M. Prado, from the Institute of Chemistry, USP, for use of the mass spectrometry facility, and Drs. A. Miranda and T.M. Domingues, from UNIFESP, for use of the circular dichroism facility. We also thank Dr. Filipe da Silva Lima for help in the preparation of Scheme 2 and Graphical Abstract. Authors are recipients of the following fellowships: M.C. Manzini, CNPq M.Sc.; T.L. Santos, CAPES Ph.D.; M.A. Rodrigues, CAPES post-doctoral; G.K.V. Saraiva, CNPq Ph.D., J.C. Bozzelli Jr., FAPESP Ph.D.; S. Schreier, I.M. Cuccovia, A.P.C. Valente, F.L.C. Almeida, M.P. Bemquerer, and H. Chaimovich, CNPq research fellowships.

References

[1] The evolving threat of antimicrobial resistance. Options for action, World Health Organization, 2012.
[2] M. Zasloff, Antimicrobial peptides of multicellular organisms, Nature 415 (2002) 389–395.
[3] J.P. Powers, R.E.W. Hancock, The relationship between peptide structure and antibacterial activity, Peptides 24 (2003) 1681–1691.
[4] M.R. Yeaman, N.Y. Yount, Mechanisms of antimicrobial peptide action and resistance, Pharmacol. Rev. 55 (2003) 27–55.
[5] K.A. Brogden, Antimicrobial peptides: pore formers or metabolic inhibitors in bacteria? Nature 238 (2005) 350–353.
[6] H. Jenssen, P. Hamill, R.E.W. Hancock, Peptide antimicrobial agents, Clin. Microbiol. Rev. 19 (2006) 491–511.
[7] L.T. Nguyen, E.F. Haney, H.J. Vogel, The expanding scope of antimicrobial peptide structures and their modes of action, Trends Biotechnol. 29 (2011) 464–472.
[8] P. Nicolas, Multifunctional host defense peptides: intracellular-targeting antimicrobial peptides, FEBS J. 276 (2009) 6483–6496.
[9] C.D. Fjell, J.A. Hiss, R.E.W. Hancock, G. Schneider, Designing antimicrobial peptides: form follows function, Nat. Rev. Drug Discov. 11 (2012) 337–351.
[10] K. Lohner, New strategies for novel antibiotics: peptides targeting bacterial cell membranes, Gen. Physiol. Biophys. 28 (2009) 105–116.
[11] H.W. Huang, Molecular mechanism of antimicrobial peptides: the origin of cooperativity, Biochim. Biophys. Acta 1758 (2006) 1292–1302.
[12] F.Y. Chen, M.T. Lee, H.W. Huang, Sigmoidal concentration dependence of antimicrobial peptide activities: a case study on alamethicin, Biophys. J. 82 (2002) 908–914.
[13] Y. Wu, K. He, S.J. Ludtke, H.W. Huang, X-ray diffraction study of lipid bilayer membrane interacting with amphiphilic helical peptides: diphytanoyl phosphatidylcholine with alamethicin at low concentrations, Biophys. J. 68 (1995) 2361–2369.
[14] K. Matsuzaki, Magainins as paradigm for the mode of action of pore forming polypeptides, Biochim. Biophys. Acta 1376 (1998) 391–400.

[15] Z. Oren, Y. Shai, Mode of action of linear amphipathic alpha-helical antimicrobial peptides, Biopolymers 47 (1998) 541-463.
[16] Y. Shai, Mode of action of membrane active antimicrobial peptides, Biopolymers 66 (2002) 236–248.
[17] K. Lohner, B. Bechinger, Detergent-like actions of linear amphipathic cationic antimicrobial peptides, Biochim. Biophys. Acta 1758 (2006) 1529–1539.
[18] R.M. Epand, S. Rotem, A. Mor, B. Berno, R.F. Epand, Bacterial membranes as predictors of antimicrobial potency, J. Am. Chem. Soc. 130 (2008) 14346–14352.
[19] R.F. Epand, W.L. Maloy, A. Ramamoorthy, R.M. Epand, Probing the "Charge Cluster Mechanism" in amphipathic helical cationic antimicrobial peptides, Biochemistry 49 (2010) 4076–4084.
[20] R.M. Epand, R.F. Epand, Bacterial membrane lipids in the action of antimicrobial agents, J. Pept. Sci. 17 (2011) 298–305.
[21] H.G. Boman, D. Wade, B. Wahlin, R.B. Merrifield, Antibacterial and antimalarial properties of peptides that are cecropin-melittin hybrids, FEBS Lett. 259 (1989) 103–106.
[22] D. Andreu, J. Ubach, A. Boman, B. Wåhlin, D. Wade, R.B. Merrifield, H.G. Boman, FEBS Lett. 296 (1992) 190–194.
[23] H. Sato, J.B. Feix, Peptide-membrane interactions and mechanisms of membrane destruction by amphipathic α-helical antimicrobial peptides, Biochim. Biophys. Acta 1758 (2006) 1245–1256.
[24] R.A. Houghten, C. Pinilla, S.E. Blondelle, J.R. Appel, C.T. Dooley, J.H. Cuervo, Generation and use of synthetic peptide combinatorial libraries for basic research and drug discovery, Nature 354 (1991) 84–86.
[25] E. Badosa, R. Ferre, M. Planas, L. Feliu, E. Besalu, J. Cabrefiga, E. Bardají, E. Montesinos, A library of linear undecapeptides with bactericidal activity against phytopathogenic bacteria, Peptides 28 (2007) 2276–2285.
[26] C.S. Alves, M.N. Melo, H.G. Franquelim, R.M. Planas, L. Feliu, E. Bardaji, W. Kowaslczyk, D. Andreu, N.C. Santos, M.X. Fernandes, M.A.R.B. Castanho, *Escherichia coli* cell surface perturbation and disruption induced by antimicrobial peptides BP100 and pepR, J. Biol. Chem. 285 (2010) 27536–27544.
[27] I.M. Torcato, Y. Huang, H.G. Franquelim, D. Gaspar, D.J. Craik, M.A.R.B. Castanho, S.T. Henriques, Design and characterization of novel antimicrobial peptides, R-BP100 and RW-BP100, with activity against Gram-negative and Gram-positive bacteria, Biochim. Biophys. Acta 1828 (2013) 944–955.
[28] R. Ferre, M.N. Melo, A.D. Correia, L. Feliu, E. Bardají, M. Planas, M. Castanho, Synergistic effects of the membrane actions of cecropin-melittin antimicrobial hybrid peptide BP100, Biophys. J. 96 (2009) 1815–1827.
[29] K. Eggenberger, C. Mink, P. Wadhwani, A.S. Ulrich, P. Nick, Using the peptide BP100 as a cell-penetrating tool for the chemical engineering of actin filaments within living plant cells, Chembiochem 12 (2011) 132–137.
[30] M. Lakshmanan, Y. Kodama, T. Yoshizumi, K. Sudesh, K. Numata, Rapid and efficient gene delivery into plant cells using designed peptide carriers, Biomacromolecules 14 (2013) 10–16.
[31] C.S. Alves, V. Kairys, M.A.R.B. Castanho, M.X. Fernandes, Interaction of antimicrobial peptides, BP100 and pepR, with model membrane systems as explored by Brownian dynamics simulations on a coarse-grained model, Biopolymers 98 (2012) 294–312.
[32] M.N. Melo, A study on the mode of action of clinically relevant antimicrobial peptides, (Ph.D. Thesis) Lisboa University, Faculdade de Ciências, Departamento de Química e Bioquímica, Portugal, 2010.
[33] P. Wadhwani, R.F. Epand, N. Heidenreich, J. Bürck, A.S. Ulrich, R.M. Epand, Membrane-active peptides and the clustering of anionic lipids, Biophys. J. 103 (2012) 265–274.
[34] P. Wadhwani, E. Strandberg, J. van den Berg, C. Mink, J. Bürcka, R.A.M. Ciriello, A.S. Ulrich, Dynamical structure of the short multifunctional peptide BP100 in membranes, Biochim. Biophys. Acta 1838 (2014) 940–949.
[35] F.A. Maximiano, M.A. Silva, K.R.P. Daghastanli, P.S. Araujo, H. Chaimovich, I.M. Cuccovia, A convenient method for lecithin purification from fresh eggs, Quim. Nova 31 (2008) 910–913.
[36] E. Ralston, L.M. Hjelmeland, R.D. Klausner, J.N. Weinstein, R. Blumenthal, Carboxyfluorescein as a probe for liposome-cell interactions. Effect of impurities and purification of the dye, Biochim. Biophys. Acta 649 (1981) 133–137.
[37] W.C. Chan, P.D. White, Fmoc solid phase peptide synthesis, Oxford University Press, Oxford, 2000.
[38] F. Albericio, Developments in peptide and amide synthesis, Curr. Opin. Chem. Biol. 8 (2004) 211–221.
[39] R. Subiros-Funosas, G.A. Acosta, A. El-Faham, F. Albericio, Microwave irradiation and COMU: a potent combination for solid-phase peptide synthesis, Tetrahedron Lett. 50 (2009) 6200–6202.
[40] M. Friedman, Application of the ninhydrin reaction for analysis of amino acids, peptides and proteins to agricultural and biomedical sciences, J. Agric. Food Chem. 52 (2004) 385–406.
[41] D. Suckau, A. Resemann, M. Schuerenberg, P. Hufnagel, J. Franzen, A. Holle, A novel MALDI LIFT-TOF/TOF mass spectrometer for proteomics, Anal. Bioanal. Chem. 376 (2003) 952–965.
[42] J.N. Weinstein, S. Yoshikama, P. Henkart, R. Blumenthal, W.A. Hagins, Liposome-cell interaction: transfer and intracellular release of a trapped fluorescent marker, Science 195 (1977) 489–492.
[43] G. Rouser, S. Fleisher, A. Yamamoto, Two dimensional thin layer chromatographic separation of polar lipids and determination of phospholipids by phosphorous analysis of spots, Lipids 5 (1970) 494–496.
[44] Y.H. Chen, J.T. Yang, K.H. Chau, Determination of helix and β form of proteins in aqueous solution by circular dichroism, Biochemistry 13 (1974) 3350–3359.
[45] D.S. Wishart, C.G. Bigam, J. Yao, F. Abildgaard, H.J. Dyson, E. Oldfield, J.L. Markley, B.D. Sykes, ^{1}H, ^{13}C and ^{15}N chemical shift referencing in bimolecular NMR, J. Biomol. NMR 6 (1995) 135–140.
[46] M. Piotto, V. Saudek, V. Sklenar, Gradient-tailored excitation for single-quantum NMR spectroscopy of aqueous solutions, J. Biomol. NMR 2 (1992) 661–665.
[47] A. Bax, D.G. Davis, MLEV-17 based two-dimensional homonuclear magnetization transfer spectroscopy, J. Magn. Reson. 65 (1985) 355–360.
[48] F. Delaglio, S. Grzesiek, G. Vuister, J. Pfeifer, A. Bax, NMRPipe: a multidimensional spectral processing system based on UNIX pipes, J. Biomol. NMR 6 (1995) 277–293.
[49] B. Johnson, R. Blevins, NMR VIEW - A Computer program for the visualization and analysis of NMR data, J. Biomol. NMR 4 (1994) 603–614.
[50] P. Schanda, E. Kupce, B. Brutscher, SOFAST-HMQC experiments for recording two-dimensional heteronuclear correlation spectra of proteins within a few seconds, J. Biomol. NMR 33 (2005) 199–211.
[51] R.F. Chen, J.R. Knutson, Mechanism of fluorescence concentration quenching of carboxyfluorescein in liposomes: energy transfer to nonfluorescent dimers, Anal. Biochem. 172 (1988) 61–77.
[52] M.I. Angelova, D.S. Dimitrov, Liposome electroformation, Faraday Discuss. Chem. Soc. 81 (1986) 303–311.
[53] T.M. Domingues, K.A. Riske, A. Miranda, Revealing the lytic mechanism of the antimicrobial peptide gomesin by observing giant unilamellar vesicles, Langmuir 26 (2010) 11077–11084.
[54] D.T. Jones, Protein secondary structure prediction based on position-specific scoring matrices, J. Mol. Biol. 292 (1999) 195–202.
[55] M. Schiffer, A.B.. Edmundson, Use of helical wheels to represent the structures of proteins and to identify segments with helical potential, Biophys. J. 7 (1967) 121–135.
[56] D.E. Eisenberg, R.M. Weiss, T.C. Terwilliger, The helical hydrophobic moment: a measure of the amphiphilicity of a helix, Nature 299 (1982) 371–374.
[57] P. Fan, C. Bracken, J. Baum, Structural characterization of monellin in the alcohol-denatured state by NMR: evidence for beta-sheet to alpha-helix conversion, Biochemistry 32 (1993) 1573–1582.
[58] A. Jasanoff, A.R. Fersht, Quantitative determination of helical propensities from TFE titration curves, Biochemistry 33 (1994) 2129–2135.
[59] S. Schreier, S.R. Barbosa, F. Casallanovo, R.F.F. Vieira, E.M. Cilli, A.C.M. Paiva, C.R. Nakaie, Conformational basis for the biological activity of TOAC-labeled angiotensin II and bradykinin, EPR, circular dichroism and fluorescence studies, Biopolymers 74 (2004) 389–402.
[60] P.F. Almeida, A.S. Ladokhin, S.H. White, Hydrogen-bond energetics drive helix formation in membrane interface, Biochim. Biophys. Acta 1818 (2012) 178–182.
[61] D.J. Gordon, G. Holzworth, Artifacts in the measured optical activity of membrane suspensions, Arch. Biochem. Biophys. 142 (1971) 481–488.
[62] D.A. Urry, Protein conformation in biomembranes. Optical rotation and absorption of membrane suspensions, Biochim. Biophys. Acta 265 (1972) 115–168.
[63] B.A. Wallace, D. Mao, Circular dichroism analyses of membrane proteins: an examination of differential light scattering and absorption flattening effects in large membrane vesicles and membrane sheets, Anal. Biochem. 142 (1984) 317–328.
[64] L.N. Medeiros, R. Angeli, C.G. Sarzedas, E. Barreto-Bergter, A.P. Valente, E. Kurtenbach, F.C.L. Almeida, Backbone dynamics of the antifungal Psd1 pea defensin and its correlation with membrane interaction by NMR spectroscopy, Biochim. Biophys. Acta 1798 (2010) 105–113.
[65] C. Cruzeiro Silva, F. Gomes-Neto, L.W. Tinoco, E.M. Cilli, P.V.R. Barros, P.A. Lapido-Loureiro, P.M. Bisch, A.P. Valente, F.C. Almeida, Structural biology of membrane-acting peptide: Conformational plasticity of anticoccidial peptide PW2 probed by solution NMR, Biochim. Biophys. Acta 1768 (2007) 182–3192.
[66] M.N. Melo, F.J. Souza, F.A. Carneiro, M.A. Castanho, A.P. Valente, F.L. Almeida, A.T. Dapoian, R. Mohana-Borges, Interaction of dengue virus fusion peptide with membranes assessed by NMR: The essential role of the envelope protein Trp^{101} for membrane fusion, J. Mol. Biol. 392 (2009) 736–746.
[67] S.A. Tatulian, Binding of alkaline-earth metal cations and some anions to phosphatidylcholine liposomes, Eur. J. Biochem. 170 (1987) 413–420.
[68] M.V. Scarpa, F.A. Maximiano, H. Chaimovich, I.M. Cuccovia, Interfacial concentrations of chloride and bromide and selectivity for ion exchange in vesicles prepared with dioctadecyldimethylammonium halides, lipids, and their mixtures, Langmuir 18 (2002) 8817–8823.
[69] B. Klasczyc, V. Knecht, R. Lipowsky, R. Dimova, Interactions of alkali metal chloride with phosphatidylcholine vesicles, Langmuir 26 (2010) 18951–18958.
[70] F. Pincet, S. Cribier, E. Perez, Bilayers of neutral lipids bear a small but signicant charge, Eur. Phys. J. B 11 (1999) 127–130.
[71] J.M. Freire, M.M. Domingues, J. Matos, M.N. Melo, A.S. Veiga, N.C. Santos, M.A.R.B. Castanho, Using zeta-potential measurements to quantify peptide partition to lipid membranes, Eur. Biophys. J. 40 (2011) 481–487.
[72] M.P. dos Santos Cabrera, D.S. Alvares, N.B. Leite, B.M. de Souza, M.S. Palma, K.A. Riske, J. Ruggiero Neto, New insight into the mechanism of action of wasp mastoparan peptides: lytic activity and clustering observed with giant vesicles, Langmuir 27 (2011) 10805–10813.
[73] V. Knecht, B. Klasczyk, Specific binding of chloride ions to lipid vesicles and implications at molecular scale, Biophys. J. 104 (2013) 818–824.
[74] J. Dufourcq, J.-F. Faucon, G. Fourche, J.L. Dasseux, M. Le Maire, T. Gulik-Krzywicki, Morphological changes of phosphatidylcholine bilayers induced by melittin: vesicularization, fusion, discoidal particles, Biochim. Biophys. Acta 859 (1986) 33–48.
[75] H. Steiner, D. Andreu, R.B. Merrifield, Binding and action of cecropin and cecropin analogues: antibacterial peptides from insects, Biochim. Biophys. Acta 939 (1988) 260–2666.
[76] M.C. Manning, M. Illangasekare, R.W. Woody, Circular dichroism studies of distorted α-helices, twisted β-sheets, and β-turns, Biophys. Chem. 31 (1988) 77–86.

[77] D. Stigter, On the adsorption of counterions at the surface of detergent micelles, J. Phys. Chem. 68 (1964) 3603–3611.
[78] C. Treiner, M.H. Mannenbach, Counterion condensation on mixed cationic/nonionic micellar systems: Bjerrum´s electrostatic condition, Colloid Polym. Sci. 268 (1990) 88–95.
[79] C. Tanford, The hydrophobic effect: Formation of micelles and biological membranes, 2nd ed. John Wiley & Sons, New York, 1980. 60–78.
[80] M. Benrraou, B.L. Bales, R. Zana, Effect of the nature of the counterion on the properties of anionic surfactants. 1. Cmc, ionization degree at the cmc and aggregation number of micelles of sodium, cesium, tetramethylammonium, tetraethylammonium, tetrapropylammonium, and tetrabutylammonium dodecyl sulfates, J. Phys. Chem. B 107 (2003) 13432–13440.
[81] F.H. Quina, H. Chaimovich, Specific ion binding at charged interfaces. I. Unified conceptual framework for micellar solutions, J. Phys. Chem. 83 (1979) 1844–1850.
[82] C. Mazzuca, B. Orioni, M. Coletta, F. Formaggio, C. Toniolo, G. Maulucci, M. De Spirito, B. Pispisa, M. Venanzi, L. Stella, Fluctuations and the rate-limiting step of peptide-induced membrane leakage, Biophys. J. 99 (2010) 1791–1800.
[83] N. Ben-Tal, B. Honig, R.M. Peitzsch, G. Denisov, S. McLaughlin, Binding of small basic peptides to membranes containing acidic lipids: theoretical models and experimental results, Biophys. J. 71 (1996) 561–575.
[84] F.A. Maximiano, H. Chaimovich, I.M. Cuccovia, Decarboxylation of 6-nitrobenzisoxazole-3-carboxylate in mixed micelles of zwitterionic and positively charged surfactants, Langmuir 22 (2006) 8050–8055.
[85] M. Mosior, S. McLaughlin, Peptides that mimic the pseudosubstrate region of protein kinase C bind to acidic lipids in membranes, Biophys. J. 60 (1991) 149–159.
[86] K. Hristova, C.E. Dempsey, S.H. White, Structure, location, and lipid perturbations of melittin at the membrane interface, Biophys. J. 80 (2001) 801–811.
[87] A.S. Ladokhin, S.H. White, "Detergent-like" permeabilization of anionic lipid vesicles by melittin, Biochim. Biophys. Acta 1514 (2001) 253–260.
[88] M. Bachar, O.M. Becker, Protein-induced membrane disorder: a molecular dynamics study of melittin in a dipalmitoylphosphatidylcholine bilayer, Biophys. J. 78 (2000) 1359–1375.
[89] A. Giangaspero, L. Sandri, A. Tossi, Amphipathic alfa-helical antimicrobial peptides, A systemic study of the effects of structural and physical properties on biological activity, Eur. J. Biochem. 268 (2001) 5589–5600.
[90] H. Leontiadou, A.E. Mark, S.J. Marrink, Antimicrobial peptides in action, J. Am. Chem. Soc. 128 (2006) 12156–12161.
[91] D. Sengupta, H. Leontiadou, A.E. Mark, S.J. Marrink, Toroidal pores formed by antimicrobial peptides show significant disorder, Biochim. Biophys. Acta 1778 (2008) 2308–2317.
[92] E. Mátyus, C. Kandt, D.P. Tieleman, Computer simulation of antimicrobial peptides, Curr. Med. Chem. 14 (2007) 2789–2798.
[93] F. Jean-François, J. Elezgaray, P. Berson, P. Vacher, E.J. Dufourc, Pore formation induced by an antimicrobial peptide: Electrostatic effects, Biophys. J. 95 (2008) 5748–5756.
[94] E.J. Dufourc, I.C. Smith, J. Dufourcq, Molecular details of mellitin-induced lysis of phospholipid membranes as revealed by deuterium and phosphorous NMR, Biochemistry 25 (1986) 6448–6455.
[95] G. Laroche, E.J. Dufourc, M. Pézolet, J. Dufourcq, Coupled changes between lipid order and polypeptide conformation at the membrane surface. A ^{2}H NMR and Raman study of polylysine-phosphatidic acid systems, Biochemistry 29 (1990) 6460–6465.
[96] J.H. Kleinschmidt, D. Marsh, Spin-label electron spin resonance studies on the interactions of lysine peptides with phospholipid membranes, Biophys. J. 73 (1997) 2546–2555.
[97] J.H. Kleinschmidt, J.E. Mahaney, D.D. Thomas, D. Marsh, Interaction of bee venon melittin with zwitterionic and negatively charged phospholipid bilayers: a spin-label electron spin resonance study, Biophys. J. 72 (1997) 767–778.
[98] W. Hartmann, H.-J. Galla, Binding of polylysine to charged bilayer membranes: molecular organization of a lipid-peptide complex, Biochim. Biophys. Acta 509 (1978) 474–490.
[99] A. Arouri, M. Dathe, A. Blume, Peptide induced demixing in PG/PE lipid mixtures: a mechanism for the specificity of antimicrobial peptides towards bacterial membranes? Biochim. Biophys. Acta 1788 (2009) 650–659.
[100] A. Mecke, D.-K. Lee, A. Ramamoorthy, B.G. Orr, M.M. Banaszak Holl, Membrane thinning due to antimicrobial peptide binding: an atomic force microscopy study of MDI-78 in lipid bilayers, Biophys. J. 89 (2005) 4043–4050.